STEADY-STATE ELECTROTRANSPORT OF CARBON IN IRON

By
TORU OKABE

A DISSERTATION PRESENTED TO THE GRADUATE COUNCIL OF
THE UNIVERSITY OF FLORIDA
IN PARTIAL FULFILLMENT OF THE REQUIREMENTS FOR THE
DEGREE OF DOCTOR OF PHILOSOPHY

UNIVERSITY OF FLORIDA
1969

ACKNOWLEDGMENTS

The author expresses his appreciation for the guidance, assistance and concern of the many individuals who contributed to the successful completion of this dissertation.

Drs. R. T. DeHoff, A. G. Guy, R. E. Hummel and J. Kronsbein, who are the members of the author's committee, provided effective guidance and counsel during the course of this investigation. Special thanks go to Dr. Guy, the chairman of the committee, for the many discussions and helpful suggestions which led to the successful performance of this work.

Dr. R. A. Oriani, E. C. Bain Laboratory for Fundamental Research of the United States Steel Corporation, and Dr. J. C. Slater, Graduate Research Professor of the Department of Physics at the University of Florida, provided valuable suggestions for the interpretation of the experimental results. Drs. H. Oikawa and R. Watanabe contributed useful discussions which provided additional stimuli for the development of the final method. Professors W. T. Tiffin and R. A. Rummel assisted the author with several aspects of the experimental work.

The United States Steel Corporation furnished high-purity carbon steel used in this investigation. The Armco Steel Corporation made the carbon analyses which were necessary for the quantitative evaluation of the results. J. Bottcher, Sperry Electronic Tube Division, helped with the palladium electroplating technique. Mrs. B. B. Higgins made

the measurements of the plated layers with the electron microprobe analyzer.

The author benefited from many discussions with his fellow graduate students during special research meetings. Notable help was obtained from Messrs. H. M. Breitling, G L. Hofman and M. I. Lifland on technical matters and from Mr. W. A. Slippy, Jr., on literary style of this dissertation.

The author's wife, Masako, contributed to his well-being and therefore to the completion of this work by her intelligence, understanding, affection and home-making.

During his student days, the author's mother, Mrs. T. Okabe, and his parents-in-law, Mr. and Mrs. Y. Amatsuji, instilled physical and spiritual strength that contributed much to the present achievement.

Mrs. M. E. Godey, Mr. P. D. Kalb, Mr. C. J. Minier, Mr. H. M. Brown, Mr. H. R. King, Mr. E. C. Logsdon, Mr. S. Senmoto and Mr. C. Wang provided the technical skills necessary for the completion of this dissertation.

The author gratefully acknowledges the support by the National Science Foundation of his research on electrotransport at the Department of Metallurgical and Materials Engineering of the University of Florida.

TABLE OF CONTENTS

		Page
ACKNOWLEDGMENTS		ii
LIST OF TABLES		vi
LIST OF FIGURES		vii
ABSTRACT		x
Chapter		
I.	INTRODUCTION	1
II.	LITERATURE REVIEW	3
III.	APPARATUS FOR ELECTROTRANSPORT	13
	The Specimen Chamber	14
	Power Supply	18
	Temperature Controller	20
	Vacuum System	22
IV.	PHENOMENOLOGICAL DESCRIPTION OF STEADY-STATE ELECTROTRANSPORT	24
V.	PRELIMINARY EXPERIMENTS	36
	Specimen	36
	Experimental Conditions	37
	Preliminary Experimental Results	37
	Carbon Gain or Loss in the Specimen During the Experiment	43
VI.	EXPERIMENTS WITH RADIOACTIVE CARBON, C^{14}	45
	Carburization	45
	Carburization of Armco Iron	45
	Homogeneity of the Carburized Specimen	48
	Surface Treatment of the Specimen	50
	Experimental Condition and Method of Electrotransport	55
	Results of the Electrotransport Experiment	60

TABLE OF CONTENTS (continued)

Chapter		Page
VI.	(continued)	
	Cooling Rate of the Specimen After the Electrotransport	60
	Confirmation of Attainment of the Steady-State	60
	Value of the Apparent Charge, Z*	64
VII.	DISCUSSION AND CONCLUSIONS	94
	Diffusion Between Steel and Electroplated Layers	94
	Experimental Errors	94
	Significance of the Investigation	99
VIII.	SUGGESTIONS FOR FUTURE WORK	101
	Experimental Apparatus and Techniques	101
	Extension of the Interstitial Electrotransport Experiment	102
Appendix		
I.	SOLUTION OF STEADY-STATE EQUATION	104
II.	GEOMETRY OF COUNTING RADIOACTIVITY	106
III.	DETERMINATION OF THE INITIAL CARBON CONCENTRATION BY GRAPHICAL METHOD	108
LIST OF REFERENCES		111
BIOGRAPHICAL SKETCH		114

LIST OF TABLES

Table		Page
2.1	Previous Works on Electrotransport of Carbon in Iron	4
2.2	Electrotransport of Interstitial Solute (except Fe-C system)	7
5.1	Chemical Analysis of Specimen Used	36
5.2	Experimental Conditions	37
5.3	Carbon Content after Electrotransport	44
6.1	Carbon Content Produced During Preliminary Carburizing Studies	47
6.2	Conditions for Carburizing of Specimen Using C^{14}	48
6.3	Carbon Content and Radioactivity of the Carburized Specimen	53
6.4	Conditions for Copper and Palladium Electrolytic Plating	54
6.5	Experimental Condition for Electrotransport of C^{14} in Iron	57
6.6 - 6.24		
	Surface Activity Measurements	66-84
6.25	The Apparent Charge, Z*, of Carbon in γ Iron	92

LIST OF FIGURES

Figure		Page
3.1	Overall view of the electrotransport apparatus	15
3.2	Specimen chamber, electrodes, and steel specimen . . .	16
3.3	Schematic wiring diagram for power supply and temperature control	19
4.1	Schematic illustration of the transport of interstitial atoms across a reference plane in the metal lattice	25
4.2	Schematic illustration of the relation between the current, I, passing through a specimen and the electric field intensity, E, existing within the metal	27
4.3	Schematic illustration of electrotransport in a sandwich-type diffusion specimen at 927°C	29
4.4	Electrotransport effects in a finite solid having an initial, uniform concentration n_o. Concentration distributions corresponding to four different times are shown, t_∞ corresponding to the steady-state	32
4.5	Theoretical carbon distribution of electrotransport in 0.5% C steel	35
5.1	Microstructure of 0.5% C steel before and after electrotransport at 927°C (slowly cooled). 100X	39
	(a) Before electrotransport	39
	(b) After electrotransport for 1 hour	39
	(c) After electrotransport for 8 hours	40
	(d) After electrotransport for 24 hours	40
5.2	Microstructure of 0.5% C steel after electrotransport at 927°C (rapidly cooled). 100X	41

Figure		Page
5.3	Carbon distribution after electrotransport (8 hours, 927°C), with copper plated specimen. The result was obtained by chemical analysis of carbon in the sectioned specimen	42
6.1	Carburization cell made of pure copper, shown with three 1mm thick specimens	46
6.2	Typical distribution of carbon in two specimens after carburizing in a $BaCO_3$ + C mixture	49
6.3	Carbon distribution at the vicinity of the surface	51
6.4	Typical microstructure of the specimen carburized with charcoal powder and barium carbonate containing C^{14}. 100X	52
	(a) 0.50 wt. %	52
	(b) 0.12 wt. %	52
6.5	Experimental procedure for the electro-transport of carbon in γ iron, employing radioactive carbon, C^{14}	56
6.6	The carbon-activity vs. the distance along the specimen. Comparison of the rapidly and slowly cooled specimen obtained from the experiment for 8 hours at 927°C with about 2,200 A/cm^2 in 0.47 wt. % carbon steel	61
6.7	Carbon distribution after electrotransport for 15 minutes to 24 hours at 927°C with 2,170 A/cm^2 in 0.47 wt. % carbon steel	62
6.8	Semi-log plots of carbon concentration vs. distance along the specimen after electro-transport for 8 to 24 hours at 927°C with 2,170 A/cm^2 in 0.47 wt. % carbon steel	63
6.9	Semi-log plots of carbon concentration vs. distance along the specimen after electro-transport for 5 hours at 977°C with 2,510 A/cm^2 (0.50 wt. % carbon steel).	85

LIST OF FIGURES (continued)

Figure		Page
6.10	Semi-log plots of carbon concentration vs. distance along the specimen after electro-transport for 3 hours at 1,027°C with 2,570 A/cm^2 (0.47 wt. % carbon steel)	86
6.11	Semi-log plots of carbon concentration vs. distance along the specimen after electro-transport for 8 hours at 927°C with 1,390 A/cm^2 (0.47 wt. % carbon steel)	87
6.12	Semi-log plots of carbon concentration vs. distance along the specimen after electro-transport for 12 hours at 927°C with 2,460 and 1,980 A/cm^2 (0.12 and 0.14 wt. % carbon steel)	88
6.13	Semi-log plots of carbon concentration vs. distance along the specimen after electro-transport for 6 hours at 977°C with 2,190 A/cm^2 (0.13 wt. % carbon steel)	89
6.14	Semi-log plots of carbon concentration vs. distance along the specimen after electro-transport for 3.5 hours at 1,027° C with 2,300 A/cm^2 (0.11 wt. % carbon steel)	90
6.15	Semi-log plots of carbon concentration vs. distance along the specimen after electro-transport for 12 hours at 927 °C with 1,100 and 1,490 A/cm^2 (0.12 wt. % carbon steel)	91
A2.1	Geometry of the measurement of surface activity of the specimen (Nuclear Chicago 480 Gas-Flow Detector)	107
A3.1	Schematic diagram for determining the initial radioactivity by a graphical method	109

Abstract of Dissertation Presented to the Graduate Council in Partial Fulfillment of the Requirements for the Degree of Doctor of Philosophy

STEADY-STATE ELECTROTRANSPORT OF CARBON IN IRON

By

Toru Okabe

December, 1969

Chairman: Dr. A. G. Guy
Major Department: Metallurgical and Materials Engineering

Electrotransport of carbon in γ iron was studied by a steady-state method. Previous experimental studies of electrotransport in solid metallic systems have been limited to the use of unsteady-state methods. The steady-state distribution in a solid system can be attained in a reasonable time provided certain conditions are fulfilled. This method has the advantage that the effective charge, Z^*, can be directly evaluated from the ratio of the chemical compositions at the anode and cathode ends without using other experimental parameters such as chemical diffusivity or electrical mobility. C^{14} was introduced into Armco iron specimens by carburizing, and the steady-state concentration-distance curve was determined by the method of residual radioactivity. The effective charge, Z^*, of carbon in γ iron under the experimental conditions employed (0.11 to 0.50 wt. % C, 927°C to 1,027°C, and 1,100 to 2,600 A/cm^2 current density) is $\pm 3.9_9$ $\pm 0.0_8$. No dependence of Z^* on carbon content, temperature, or current

density was detected. The results were interpreted as showing that the fully-ionized carbon ion, C^{4+}, is driven only by the electric field force, and that electronic carriers have a negligible effect.

CHAPTER I

INTRODUCTION

When an electric field is applied to a pure metal or alloy in the liquid or solid state, a significant transport of specific atomic components occurs, in addition to the transport of charge carriers (i.e., electrons and "holes"). This process of mass transport of ions is sometimes referred to as "electromigration," "electrodiffusion," or "electrotransport." The first known observation of electrotransport in metals is attributed to Gerardin,[1] who noticed that after electrolysis of a lead-tin alloy in the molten state, the sample became soft at one end and brittle at the other. In addition, he also found that a sodium-mercury alloy would decompose water only at one end. The motion of a specific atomic component in an alloy or pure metal may be directed toward the anode (+) or the cathode (-), depending on such factors as type of alloys, alloy composition, temperature, current density, etc. The phenomenon of electrotransport has been the subject of numerous investigations and publications since the early 1930's when several investigators experimentally demonstrated electrotransport in solid metals when sufficiently high current densities and temperatures were used.

The research presented in this dissertation deals with the electrotransport of carbon in iron. It is significant in demonstrating for the first time that the steady-state condition can be attained in

solid metallic systems in a reasonable time provided certain conditions are fulfilled. The study of electrotransport of an interstitial atom, such as carbon in iron, is especially interesting because the mechanism of transport is relatively simple compared with the vacancy mechanism in substitutional alloys. At present it seems unlikely, although proposed recently by Sidorenko,[2] that the vacancy mechanism may take place in the electrotransport of an interstitial atom such as hydrogen in iron. The carbon atom in the Fe-C system can be pictured as merely jumping from one interstitial position to a neighboring one in the essentially rigid framework of the iron lattice. Correlation effect can be neglected. Also, the electronic configuration of an interstitial atom, such as carbon, can be determined more easily than that of elements with a more complex electronic structure, such as the transition elements.

It must be emphasized that all previous experiments on the electrotransport of metals and alloys have been conducted using the conventional unsteady-state methods.[3] Although the mathematical relations for possible steady-state procedures are well known,[4] only studies of rapidly diffusing gases in metals[5] have been reported in the literature. The present research makes full use of the fact that the ordinary diffusion coefficient, D, does not enter into the quantitative determination of the effective charge, Z*, the essential parameter of electrotransport. The use of radioactive carbon, C^{14}, for determining the concentration-distance curves after electrotransport gave more precise data than could have been obtained using ordinary chemical methods.

CHAPTER II

LITERATURE REVIEW

Since the steady-state condition has not been achieved in solid metallic systems by any previous investigator, the following literature survey pertains to the usual, unsteady-state results in Fe-C and related interstitial systems. The first studies were made over thirty years ago[6] and, although numerous investigations have been reported since that time,[7] the essential nature of electrotransport in this system remains unclear. The earlier investigators[6,8-12] believed that their results indicated a charge of +4 (or less) on the carbon ions, but recent studies[2,3,13-17] suggest that effects in addition to simple electrostatic interaction are involved. Kovenskii[14] obtained effective charges, Z*, on the order of +10, which he attributed to the effect of the "hole wind."

Bibby and coworkers[16] used a microhardness technique to determine the concentration-distance curve for electrotransport of carbon in austenite. They found that Z* for carbon decreased with temperature from about +13 at 902°C to +9 at 950°C. In a continuation of this study,[18] Bibby and Youdelis investigated the electrotransport of carbon in ferrite in a Hall field using a phase-boundary-migration technique. The Hall field should permit the determination of the true charge on the ions. A value of +4.3 was found for carbon at 752°C. Table 2.1 summarized the previous research on electrotransport of carbon in iron.

Table 2.1

Previous Works on Electrotransport of Carbon in Iron

Investigator	Specimen Length (cm)	Specimen Diameter (mm)	Specimen Type	Carbon Content (wt. %)	T (°C)	t (hr.)	Atmosphere
W. Seith[6] (1935)	30	1.5	2 phase zone 1cm	~1.0	1,065	10~25	Vac. ~10^{-4}
P. Dayal[8] (1950)	2.5	OD 9.5 ID 5.0	1 phase	0.46 1.10	1,000 ~1,200	~10	nitrogen
I. N. Frantsevich[10-11] (1957)	6	0.6	zone 0.5~2cm	1.0 (?)	950 ~1,150	2~20	argon
I. F. Babikova[12] (1957)	5	5~8 x 0.08~0.15	2 phase zone I~5mm	?	530 ~800	20 min ~4 h	Vac. ~10^{-5}
N. V. Doan[17] (?)	1	?	homo-geneous	1.0	1,000	10	?
D. F. Kalinovich[13] (1961)	?	?	zoned	?	950 ~1,150	?	argon
I. I. Kovenskii[14] (1963)	?	?	zoned	0.5	950 ~1,400	?	?
M. J. Bibby[16] (1966)	>1 (?)	1.2	2 phase	0.4	842 ~950	4	Vac.
M. J. Bibby[18] (1966)	25	5 x 2.5	2 phase	0.5	752	24	?
D. F. Kalinovich[15] (1967)	7	0.5	zoned 1cm	0.6	800 ~1,400	?	Neutral Atm.

Table 2.1 (Extended)

Current Density (A/cm^2)	Mobility $cm^2/(sec \cdot v) \times 10^4$	Transport Number $(g \cdot ion/F) \times 10^6$	Effective Charge	Methods
1,100 ~1,500	0.22	---	---	Only the mobility was measured.
2,000	0.2~0.6 ~0.5	2.4~5.7 ~13	+3.5 +3.7	The mobility was computed from the amount of mass transfer across the central plane.
120 ~250	---	3.38~13.27	+1.4	The displacement of carburized zone borders was used.
1,500 ~2,200	---	6.7×10^{-2} 5.8×10^{-2}	+3.5 ~+4.5	The difference of the area in diffusion curve of the cathode and anode side was used.
590	---	---	+11	?
?	---	---	+13.4 ~+8.1	v (=UE) was measured and Z* was evaluated.
?	---	---	+10.8 ~+8.7	Same as above (also true charge, Z = +3.8 was evaluated by calculation).
?	0.02~0.0003	---	+13.5 ~+8.5	$v = (x_2 - x_1)/2t$ was measured from the boundary migration.
?	0.8	---	+4.3	Experiment under 18kOe Hall field.
?	---	0.33~17.7	---	v was determined from the velocity of the zone boundary.

A number of recent investigations have been reported on systems analogous to Fe-C. Oriani and Gonzalez[5] studied electromigration of hydrogen and deuterium in iron and nickel by a steady-state method. Z* was positive and was larger for the deuterium isotope. Momentum transfer between electron holes and the activated complex was the main cause of transport. Sidorenko and Kripyakevich[2] found Z* values on the order of +5 for electrotransport of hydrogen in α-iron and suggested a mechanism involving a hydrogen-vacancy complex. Further, they expanded their studies on the electrotransport of hydrogen to systems such as 18-8 stainless steel and copper at 700° to 1,000°C[2] and to iron, nickel and copper at temperatures as low as 40-80°C.[2] The results at high temperatures were explained in terms of the interaction between hydrogen atoms, vacancies and electrons. However, at lower temperatures, the vacancy mechanism is not involved. A summary of the quantitative results on electrotransport of interstitial alloys up to the end of 1965 has been presented by Seith[19] and Heumann.[20] The summary of the foregoing results, combined with additional recent results, other than the Fe-C system, are given in Table 2.2. In these experiments, the change of concentration after electrotransport has been analyzed by chemical analysis, radioisotopic tracer techniques, electrical resistivity measurements, metallographic techniques (boundary migration), etc.

Hehenkamp[21] has investigated the diffusion and electromigration of carbon in cobalt. Values for the frequency factor and activation energy of diffusion and effective charge of carbon were derived from the chemical diffusion of carbon in cobalt. The effective charge of carbon is appreciably larger than 4 and is temperature dependent.

Table 2.2

Electrotransport of Interstitial Solute
(except Fe-C system)

Alloy	Concentration of Interstitial (At. %)	Temperature (°C)	Mobility $cm^2/(sec\ V)x10^4$	Transfer Number $(g\cdot ion/F)x10^6$	Effective Charge or Direction of Migration	Investigator
Fe-N	---	930	0.03	---	anode	W. Seith[23] (1938)
	1.6	922~1,000	0.05~0.09	---	-13.5 ~ -8.1	M. J. Bibby[16] (1966)
Fe-B	---	1,040	0.1	---	cathode	W. Seith[23] (1938)
Fe-H	---	410~600	---	---	cathode	O. D. Gonzalez[24] (1965)
	---	441~550	---	---	~+0.23	R. A. Oriani[5] (1967)
	---	600~850	---	---	~+5	V. M. Sidorenko[2] (1968)
	---	40~80	---	---	The direction depends on temperature.	V. M. Sidorenko[2] (1969)
Fe-D	---	410~600	---	---	cathode	O. D. Gonzalez[24] (1965)
	---	463~536	---	---	~+0.38	R. A. Oriani[5] (1967)
Pd-H	2.8 2.0	182~240	1.5~2.8	---	+1	C. Wagner[25] (1940)

Table 2.2 (continued)

Alloy	Concentration of Interstitial (At. %)	Temperature (°C)	Mobility $cm^2/(sec\ V) \times 10^4$	Transfer Number $(g \cdot ion/F) \times 10^6$	Effective Charge or Direction of Migration	Investigator
Zr-O	5	1,432~1,780	---	---	anode	J. H. deBoer[26] (1940)
Ti-O	2	1,130~1,380	8~50	---	anode	F. Claisse[27] (1956)
Y-C	(~700 ppm)	1,235~1,460	0.56~3.6	---	-0.5 ~ -1.1	O. N. Carlson[22] (1966)
Y-O	(~1,000 ppm)	1,235~1,460	0.86~3.2	---	-1.1 ~ -1.8	
Y-N	(~500 ppm)	1,235~1,460	0.5~2.3	---	-2.1 ~ -0.9	
Y-H	(~100 ppm)	775~950	0.66~1.8	---	-0.9 ~ -0.26	
Co-C	0.25~0.6	800~1,300	---	---	+10 ~ +6	Th. Hehenkamp[21] (1966)
	0.5	600~1,400	---	1.3×10^{-3}~1.0	---	D. F. Kalinovich[15] (1967)
Th-C	(700 ppm)	1,440~1,675	1.2~7.4	---	-2.1 ~ -3.8	D. T. Peterson[28] (1966)
Th-N	(600 ppm)	1,480~1,685	7.0~12.5	---	-4.4 ~ -2.6	
Th-O	(325 ppm)	1,450~1,680	8.3~27.0	---	---	

Table 2.2 (continued)

Alloy	Concentration of Interstitial (At. %)	Temperature (°C)	Mobility $cm^2/(sec\ V) \times 10^4$	Transfer Number $(g \cdot ion/F) \times 10^6$	Effective Charge or Direction of Migration	Investigator
V-C	(600 ppm)	1,650~1,825	10~50	---	~+1.2	J. C. Warner[29] (1966)
V-N	(900 ppm)	1,650~1,825	3.7~7.5	---	~+1.5	
V-O	(600 ppm)	1,650~1,825	7~16	---	+1.4 ~ +1.0	
Ni-H	---	510~630	---	---	cathode	O. D. Gonzalez[24] (1965)
	---	447~625	---	---	+0.61 ~ +0.52	R. A. Oriani[5] (1967)
	---	40~80	---	---	The direction depends on temperature.	V. M. Sidorenko[2] (1969)
Ni-D	---	510~630	---	---	cathode	O. D. Gonzalez[24] (1965)
	---	482~645			+0.76 ~ +0.67	R. A. Oriani[5] (1967)
Ni-C	0.5	600~1,400	---	2.25×10^{-4} 4.45×10^{-1}	---	D. F. Kalinovich[15] (1967)
Lu-C	8mc C^{14}/g	1,330~1,600	0.2~0.5	---	-2.4 ~ -5.8	D. T. Peterson[30] (1969)
Lu-N	(500 ppm)	1,300~1,600	0.7~2.2	---	-3.2 ~ -5.7	
Lu-O	(720 ppm)	1,330~1,600	2.7~7.1	---	-2.9 ~ -2.3	

Table 2.2 (continued)

Alloy	Concentration of Interstitial (At. %)	Temperature (°C)	Mobility $cm^2/(sec\ V)x10^4$	Transfer Number $(g \cdot ion/F)x10^6$	Effective Charge or Direction of Migration	Investigator
Cu-H	---	40~80	---	---	The direction depends on temperature.	V. M. Sidorenko[2] (1969)
	---	700~1,000	---	---	anode	V. M. Sidorenko[2] (1969)
18-8 stainless steel-H	---	700~1,000	---	---	The direction depends on electric current density	V. M. Sidorenko[2] (1969)

Carlson et al.[22] determined the electrotransport velocities of carbon, oxygen and nitrogen in yttrium in the temperature range of 1,235° to 1,460°C. Diffusion coefficients and effective charges, Z*, were calculated for these elements for the same temperatures. The results for carbon, for instance, are $D = 1.40 \times 10^{-5}$ cm^2/sec and $Z^* = -0.5$ at 1,235° C, as shown in Table 2.2.

D. T. Peterson et al.[31] measured the velocity of migration of carbon, nitrogen and oxygen in thorium metal. All three species migrated in the same direction as the electron flow. The specimens were rods 6.5 cm long and 0.25 cm in diameter. The authors concluded that electrotransport should be capable of reducing the oxygen, nitrogen and carbon content in thorium to much less than 1 ppm. In these experiments these low concentrations were approached only for nitrogen, and it appears that contamination was introduced either from the vacuum atmosphere or the tantalum adapter used. The most recent paper in this series is by Schmidt and Warner,[32] which reports studies of the electrotransport of carbon, nitrogen and oxygen in vanadium. In this case, the direction of migration was opposite to that of the electron current.

It is interesting that Soviet research workers have been investigating the possibility of applying electrotransport to various commercial metallurgical processes. The following two examples involve the Fe-C system. Tkachenko[33] investigated the effect of a direct current on the process of graphitization of cast iron. He reported that the number of centers of graphitization increased under certain conditions, but the effect was a small one and of doubtful significance. Kalinovich et al.[34] found that the process of carburization of iron can be

accelerated by a factor of 2 by the use of a current density of 2,000 amp/cm^2. As in most other cases of possible commercial uses of electrotransport, this application would be uneconomic.

CHAPTER III

APPARATUS FOR ELECTROTRANSPORT

Although equipment of various designs are used for the study of electrotransport, the "vertical" type was chosen. This is the same as the electrotransport device being used by Professor Th. Heumann (Director, Institute of Metallurgical Research, Munster, Germany).

It is convenient to describe the apparatus built in terms of the four components essential to any device for the study of electrotransport as follows:

1) The specimen chamber, which serves to maintain a vacuum (10^{-5} to 10^{-6} torr) inside and to allow passage of a heavy current through the specimen;

2) The power supply, which must be capable of supplying a current on the order of 1,000 amperes at a few volts potential difference across the specimen, and must permit close continuous control of the current in response to changes in the temperature of the specimen;

3) The temperature controller, which monitors the temperature of the specimen and furnishes the electrical signals for controlling the current;

4) The vacuum system, which is necessary in order that the specimen can be kept under vacuum and can thus be protected from oxidation or contamination of its surface.

Each of these components of the apparatus will now be described in some detail in the following section.

The Specimen Chamber

A photograph of the main piece of equipment is shown in Fig. 3.1. Support is supplied by a heavy steel frame which is about 6 feet high. This frame supports two electrodes, the anode and cathode. The bottom electrode is rigidly fixed to a steel table and the steel table can be adjusted with respect to the frame. These adjustments enable the lower electrode to be maintained in a true vertical position. The lower electrode is bolted directly to the positive bus bar through the table and is adequately insulated from the main frame by teflon washers. The electrodes are cooled by water with a water jacket to protect the "O" ring seal as is shown in Fig. 3.2. Brass discs, which support the Pyrex container, are soldered to the lower electrode (Fig. 3.2). The electrode tips are truncated cones of copper with the truncated portion 10mm in diameter and with a 3mm diameter clearance hole to align the specimen and the graphite rings (Fig. 3.2). A chromel-alumel thermocouple (B.S. 30; diameter 0.254mm) tip is spot-welded on the side wall of the steel specimen. Thermocouple wires are introduced through the inlet on the side wall of Pyrex container (shown on the right side in Fig. 3.2).

Adjustment, insertion and removal of a specimen and the graphite discs are facilitated by the vertical movement of the top electrode. The top electrode is attached to, but insulated from, the roller guides.

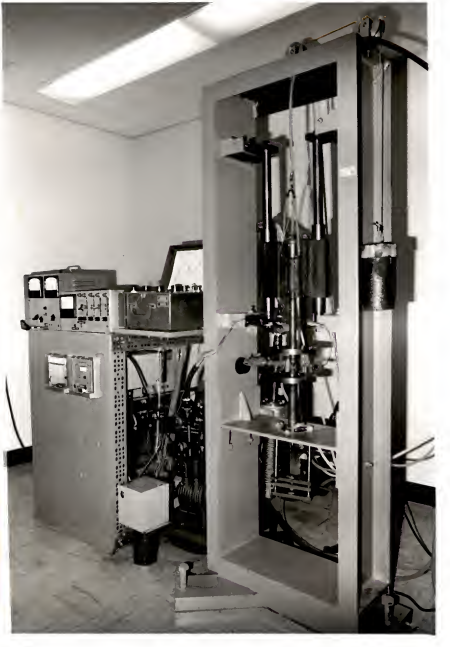

Figure 3.1. Overall view of the electrotransport apparatus.

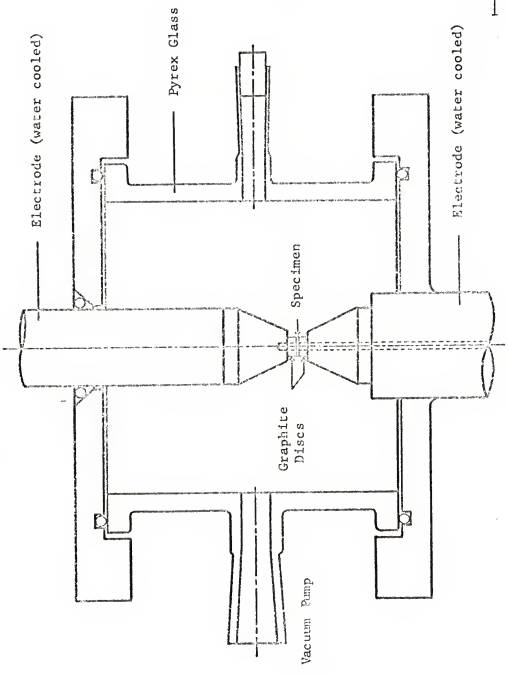

Figure 3.2. Specimen chamber, electrodes, and steel specimen.

In the connection between the top electrode and roller guides, set screws are used to permit fine adjustment of the electrode and thus alignment of both electrodes. The top electrode is also equipped with a water jacket. By means of flexible conductors the bus bar is connected to the top electrode, permitting complete vertical motion of the assembly.

Referring back to Fig. 3.1, the roller guide assembly is seen to be connected to the frame by means of leveling brackets. These leveling brackets provide the coarse alignment of the electrodes with the fine adjustment being obtained in the electrode-roller guide assembly as noted previously. The entire roller guide assembly is counter weighted to the extent that the roller guide assembly can be maintained in any position within the limits of its vertical displacement.

The main working area, i.e., the Pyrex vacuum chamber (Fig. 3.2), is a cylinder 100mm in diameter and 100mm in height with a 6mm wall thickness. There are two orifices on the side wall; one to the vacuum system and the other for the insertion of thermocouple wires. The Pyrex cylinder is capped with the same kind of brass disc mentioned previously, in which clearance holes were cut to allow the passage of the electrodes and connection to the vacuum line. The electrode holes are tapered to allow the "O" ring to seat and seal. The function of "O" ring seating brackets is to allow proper positioning of the "O" rings and is not for compression. Sealing pressure on the "O" rings is obtained by the pressure difference across them which forces the "O" rings to fill the void between the chamber, the discs and the electrode.

A typical specimen is about 1mm thick by 6mm in diameter. It contains a central hole (3mm in diameter) to align concentrically the graphite discs at the two ends of the specimen. Graphite discs (the same diameter as the specimen and 1 to 3mm thick) are used for the purpose of heating the specimen at adequate current densities and for controlling the temperature gradient. The surface of a steel specimen is first plated with copper (~10μ) to prevent loss of carbon and then plated with palladium (~10μ) to prevent the evaporation of copper during the experiment. The experiment was carried out at temperatures near 1,000°C and the current was about 300 to 500 amperes, corresponding to a current density of 1,100 to 2,600 A/cm^2.

Power Supply

A wiring diagram for the power supply is shown in Fig. 3.3. The main input to the system is a 3 phase, 208 volt, 60 amp service. In following the current through the system the first piece of apparatus encountered is the line breaker relay. This relay contains a 110V AC coil and the contacts are rated at 100 amps at 250 volts. The relay is used in the normally-closed position with current needed in the coil to keep the contacts closed.

The second pieces of apparatus the current encounters are the saturable reactors. A saturable reactor is a device by which a large output is controlled by a small input. In this case the control signal saturates the core, and the large output is the AC power source to the specimen. The saturable reactor is connected in series with the specimen

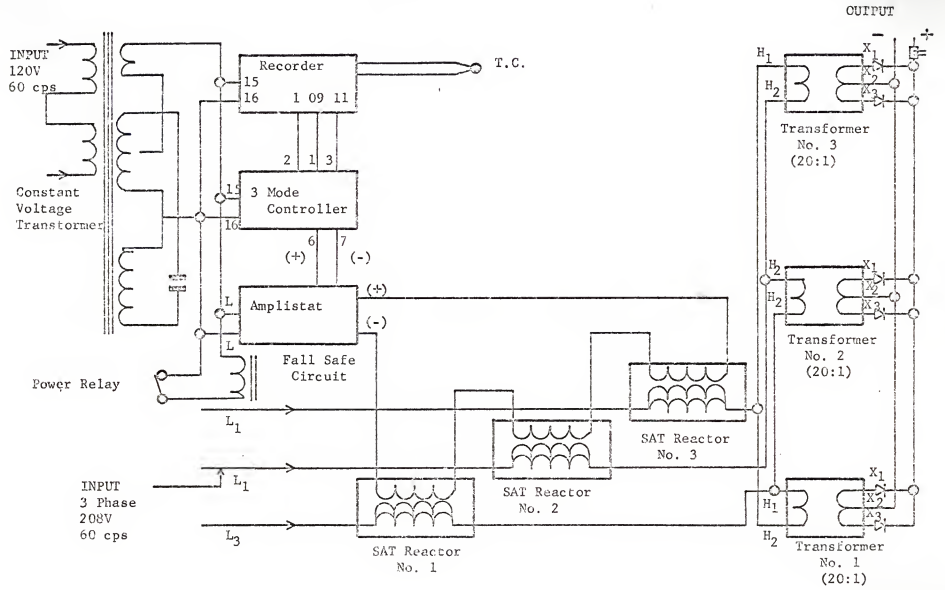

Figure 3.3. Schematic wiring diagram for power supply and temperature control.

and acts as a valve regulating the amount of power flowing into the specimen. The control windings on the saturable reactors are activated by a 75V DC, 2 amp signal. The next elements in the current path are three 20:1 step-down transformers. Each of these transformers is rated at 3 KVA with a 220V AC primary and 6.28V AC secondary, with 3.14V AC secondary to the center tap. The secondary consists of three leads labeled X_1, X_2, and X_3 on Fig. 3.3. The voltage between X_1 and X_3 is 6.28V AC and that between X_1 and X_2 is 3.14V AC as mentioned above.

Connected directly to the secondary taps X_1 and X_3 of the transformer are silicon diodes. These diodes have a maximum peak inverse voltage rating of 100 volts; a maximum DC current capacity of 350 amps and are capable of taking a maximum peak surge current of 7,000 amps. The diodes in the configuration employed give 1/6 wave rectification, which is quite suitable for the application.

The last piece of apparatus in the current path prior to the specimen is a 1,500 amp, 50 mv shunt. The signal from this shunt indicates the current flowing and also activates the current safety mechanism, which will be described later.

Temperature Controller

The temperature of the specimen is detected by a chromel-alumel thermocouple welded to the specimen. The temperature-control systems are the instruments in the upper left hand corner of Fig. 3.3. The recorder is a G. E. type 520 which is a strip-chart, single pen, ink-type instrument. It is a general purpose, servo-operated, null-

balanced recorder, equipped with a measurement slide wire. The measurement slide wire is employed to signal the "error" between the set point and measured variable, in this case between the emf of the set point and that of the thermocouple. The output of the recorder is proportional to the temperature deviation from the set point, the slide wire is part of a bridge circuit, the other part of which is located in the three-mode controller.

The controller is a G. E. type 524 three-mode controller, i.e., it has automatic proportional, reset and rate control modes. The function of the controller is to provide a 10 to 50 ma control signal for a final control element. The output of the controller is directly proportional to the unbalance of the bridge circuit and provides a DC control signal to the amplistat.

In this application the amplistat is used to amplify the output of the controller to a level large enough to serve as a control signal to a saturable reactor. The amplistat is a G. E., 150 VA, process-control type and combines a rectifier and saturable core in a self-saturating circuit. It is energized with a 120V AC source (stabilized by a constant voltage transformer) which is put through a rectifier. The output current of the rectifier serves two functions: 1) It provides the bulk of the amplistat core saturation (self-saturating), and 2) it serves as the output signal of the amplistat. Complete core saturation or "the balance of power" is supplied by the DC control signal of the controller. When the core saturates, the impedence of the output windings and the induced AC voltage are practically eliminated, permitting a large direct current to flow.

A current-safety device is installed which allows setting an upper limit on the current. This component was incorporated to protect the electrical components from overload and possible damage. The circuit is activated by a 120V AC source which passes through a 10:1 step-down transformer and through a diode bridge rectifier with a resistor-capacitor filter. The final output between points A and B is 12V DC which supplies the power input to the Magsense Meter monitor. The signal input to the Magsense unit is from the 1,500 amp, 50 mv shunt in series with the positive bus bar. A capacitor is placed across the input signal to filter out any stray AC signal. The Magsense is basically the same as a capacitor in that when the voltage across the plates of a capacitor exceeds some value, a breakdown occurs and the capacitor becomes conducting. In the Magsense unit employed, the breakdown voltage can be varied from 0 to 50 mv, i.e., the limit of the shunt output. Thus when the capacitor of the Magsense circuit "fires," the 12V DC relay is activated and in turn cuts off the power to the line-breaker relay and shuts off the main power supply. The circuit of the Magsense unit is such that once the power is shut off it must be turned on again manually by use of the reset button.

Vacuum System

The specimen chamber, as previously described, is rather small in size, and therefore standard vacuum equipment could be employed. A Welch duo-seal, model 1405B fore pump was used, which has an ultimate vacuum of 10^{-4} mm Hg (measured by a McLeod gage) and a free-air

displacement of 58 liters/min. A 2" CVC oil-diffusion pump is used to obtain the high vacuum. Mounted directly atop the diffusion pump is an air-cooled baffle and atop the baffle is a 2" gate valve. The use of the large baffle and gate valve makes it possible to take full advantage of the pumping speed of the system. All other valves are CVC high-vacuum valves, type VRA-1", with manual operators. Two thermocouple gauges are installed. These are calibrated in microns and indicate from atmospheric pressure down to a few microns. These thermocouple gauges allow the monitoring of the high and low side of the diffusion pump and are mainly used during the roughing stage. An ion gauge is located just before the chamber and is sensitive only to pressures lower than 10^{-3} torr. A vacuum of 10^{-5} to 10^{-6} torr can be maintained in the chamber.

CHAPTER IV

PHENOMENOLOGICAL DESCRIPTION OF STEADY-STATE ELECTROTRANSPORT

There are three principal "driving forces" for transport of the constituents of solid materials: a chemical gradient, a temperature gradient and an electric field. In the present research the specimen was maintained at essentially constant temperature and therefore thermo-diffusion need not be considered. There is an advantage in first treating the phenomena of electrotransport (plus diffusion) and reserving for later a consideration of the interesting theoretical conclusions that can be deduced from the experimental data.

The treatment of interstitial systems is greatly simplified by the fact that the transport of the lattice ions can be neglected in comparison to the much more rapid transport of the interstitial ions. In the Fe-C system the carbon can be pictured as jumping in the interstitial spaces (and available vacancies) in the essentially fixed iron lattice, Fig. 4.1. The iron lattice can be used as the basis for fixing a reference plane with respect to which the electrotransport of carbon is measured. There are only three essential quantities that enter into a phenomenological description of the electrotransport of an interstitial species: the concentration, n, of interstitial atoms; the electric field intensity, E; and an empirical coefficient, U, termed the electric mobility that relates the observed average velocity, v

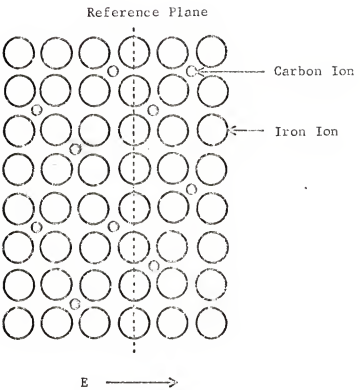

Figure 4.1. Schematic illustration of the transport of interstitial atoms across a reference plane in the metal lattice.

(cm/sec), of an interstitial atom to the field:

$$v = UE. \tag{4.1}$$

The flux of interstitial atoms is the product,

$$J_E = vn. \tag{4.2}$$

Therefore, a convenient phenomenological description of interstitial electrotransport is

$$J_E = nUE \tag{4.3}$$

where J_E is the number of atoms crossing 1 cm^2 of the reference plane per second, n is the concentration of interstitial component in atoms/cm^3, U is the electric mobility in cm^2/(sec volt), and E is the electric field intensity in volt/cm.

The electric field intensity, E, is used in the phenomenological description (rather than the experimentally measured current, I) to have a close link to theory. Since charged particles (ions, electrons and holes) are involved in the process of electrotransport, a basic equation in the theory is (see Fig. 4.2)

$$F = qE \tag{4.4}$$

which gives the force, F, exerted on a (positive) charge, q, by the field, E. If MKS units are employed, the conversion from E to the usual electrical potential, V (measured in volts), is especially convenient. Like any other potential, V is related to the force field,

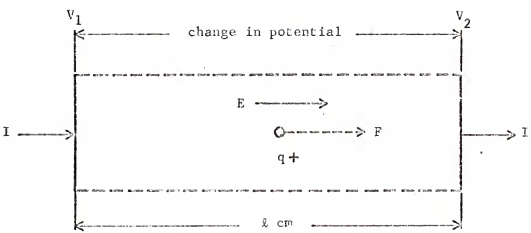

Figure 4.2. Schematic illustration of the relation between the current, I, passing through a specimen and the electric field intensity, E, existing within the metal.

E, by the general equation,

$$V = -\int E \, dx, \tag{4.5}$$

or

$$E = -\frac{dV}{dx}. \tag{4.6}$$

If it is assumed that E is constant throughout the specimen, then

$$E = \frac{V}{\ell} \tag{4.7}$$

where V is the voltage drop of conventional sign measured across some convenient length, ℓ, of the specimen. In practice, V is usually calculated from Ohm's law employing the known values of current, I, and resistance, R, of length, ℓ, of the specimen. Since $V = IR$, Eq. (4.7) can be written

$$E = \frac{IR}{\ell} \tag{4.8}$$

and it is this experimental quantity that can be pictured in Eq. (4.3).

Most experiments that have been performed to determine U, the electric mobility, involve simultaneous chemical diffusion. For example, Fig. 4.3 shows the type of effect that is produced when electrotransport of carbon in iron is superimposed on diffusion in a sandwich-type specimen. During heating in the absence of the electric field, the carbon diffuses into the iron symmetrically across the left- and right-hand interfaces. A given concentration, for example n = 0.1% C, will be found at a distance x_o from the original interface (weld interface), x = 0. On the other hand, if an electric field is applied to the specimen during the diffusion anneal (at 927° C, for

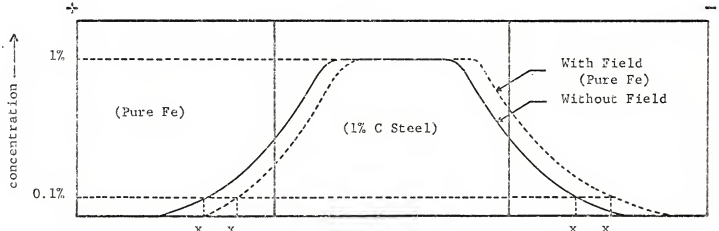

Figure 4.3. Schematic illustration of electrotransport in a sandwich-type diffusion specimen at 927° C.

example), then the concentration n = 0.1% C occurs at a different distance, x_1, on the left-hand side and at x_2 on the right-hand side. The shifting of the two curves by the distance $x_o - x_1 = x_o - x_2$ is easily understood in terms of Eq. (4.1). The electric field has imparted an average velocity, v = UE, to the carbon atoms, and each carbon atom in the specimen exhibits this velocity (in addition to the random jumping responsible for the diffusion curve in the absence of the electric field). The value of the electric mobility, U, can be calculated from the experimental data as follows:

$$U = \frac{x_o - x_1}{tE} \tag{4.9}$$

where t is the time of the experiment in seconds.

In a bar of finite length, having an initial uniform concentration, n_o, of interstitial solute, Fig. 4.4, special effects occur at the two ends. Every interstitial ion tends to acquire a velocity, v, as the result of an applied electric field, E. Therefore, after a short time, t_1, of electrotransport the solute is depleted at the left-hand end of the specimen and accumulates at the right-hand end. It is important to note that the central portion of the specimen experiences simply a uniform transport during electrotransport for a time that is short in relation to the length of the specimen (described quantitatively by Eq. (4.12) below). The analysis of the results of the experiment of Fig. 4.3 was simple because the specimen could be treated as an infinite solid and the effects of the two ends could be ignored. The total flux was the sum,

$$J = J_E + J_C = nUE - D\frac{\partial n}{\partial x}\ , \tag{4.10}$$

of the flux J_E due to electrotransport, Eq. (4.3), and flux J_C due to diffusion. Since the shape of the concentration distribution in the infinite solid is not affected by the electrotransport, the effect due to electrotransport is easily determined by simply subtracting the known distribution attributable to diffusion; i.e., by shifting the curve.

In the case of an initially uniform finite solid, Fig. 4.4, the situation is quite different. In the absence of an electric field no redistribution of the carbon atoms would occur by diffusion since there is no concentration gradient. The diffusion of the interstitial atom is called into play simultaneously with the action of electrotransport. Equation (4.10) is still the basic description of the redistribution of concentration that occurs, but the general solution is relatively complicated,[4] as can be judged by the four calculated curves shown in Fig. 4.4. An experimental determination of one of the unsteady-state curves, such as curve t_1, can be used, however, to determine the electric mobility, U, provided the diffusion coefficient, D, is known.

A more convenient and sensitive method involving a finite specimen is based on the steady-state concentration distribution, curve t_∞ in Fig. 4.4. In this case the effects of electrotransport and of diffusion are everywhere equal and opposite so that $J = 0$ in Eq. (4.10). The resulting equation is,

$$D\frac{\partial n}{\partial x} = nUE \tag{4.11}$$

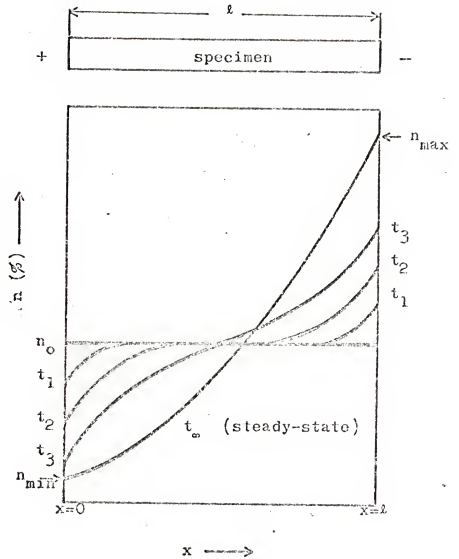

Figure 4.4. Electrotransport effects in a finite solid having an initial, uniform concentration n_o. Concentration distributions corresponding to four different times are shown, t_∞ corresponding to the steady-state.

This relation is applicable only after the specimen has passed through the unsteady-state portion of the transport process, the time for which can be estimated using the relation,[35]

$$\Delta = \exp - \frac{\pi^2 Dt}{\ell^2} \tag{4.12}$$

where Δ is the departure from the steady-state condition in a specimen ℓ cms long given a diffusion treatment for t secs. The steady-state is considered to be achieved when $\Delta = 0.01$ or less. With $D = 1.6 \times 10^{-7}$ cm^2/sec for the diffusion of carbon in austenite at 927° C[36] and $\ell = 0.1$ cm, the time for reaching the steady-state condition is 8 hours.

The electrical mobility is related to the effective charge, Z*, by the equation[7] (4.13)

$$U = \frac{DeZ^*}{kT} \tag{4.13}$$

where k is the Boltzmann constant, and e the charge of an electron. Introducing the parameter,

$$S = \frac{UE\ell}{D} , \tag{4.14}$$

it follows from Eq. (4.13) that,

$$S = \frac{E\ell eZ^*}{kT} \tag{4.15}$$

Now, for a specimen having an initial uniform concentration, n_o, the solution of Eq. (4.11) (see Appendix I) is

$$n = \frac{n_o}{(1/S)(e^S - 1)} \; e^{\frac{S}{\ell} x} \quad ; \tag{4.16}$$

the assumption has been made that Z* is independent of carbon concentration. Steady-state curves for three values of S are shown in Fig. 4.5 for ℓ = 0.1 cm. Consequently, the concentration distribution at the steady-state can be described in terms of Z* only and is independent of the ordinary D value. For this reason, the steady-state method offers the possibility of determining especially precise values of Z*.

The choice of ℓ = 0.1 cm for the thickness of the specimen is of crucial importance for two reasons. Equation (4.16) shows that the range of concentration produced at the steady-state condition increases approximately linearly with S and therefore with ℓ. In a specimen thicker than 3mm, the maximum carbon concentration would be above the solubility of carbon in austenite at 927°C. Secondly, the time to reach the steady-state condition is proportional to ℓ^2. With ordinary specimens a few centimeters in length, a prohibitively long time would be required to achieve the steady-state.

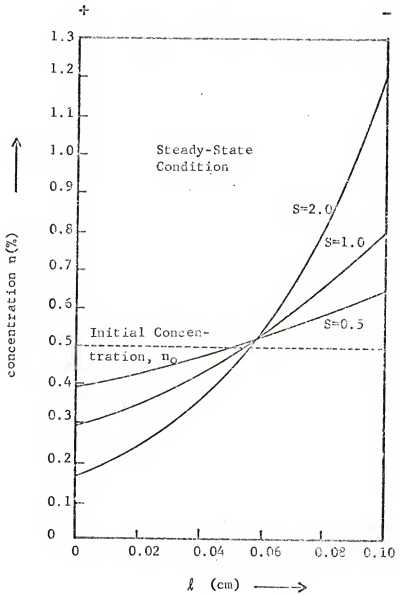

Figure 4.5. Theoretical carbon distribution of electro-transport in 0.5% C steel.

CHAPTER V

PRELIMINARY EXPERIMENTS

Specimen

In the preliminary experiments, a high-purity Fe-C alloy (obtained from the U. S. Steel Research Laboratory) was used. The chemical analysis was as follows:

Table 5.1

Chemical Analysis of Specimen Used

Elements	wt. %	Elements	wt. %
C	0.52	Cu	0.005
Mn	0.009	Ni	0.039
P	0.001	Cr	0.005
S	0.025	N	0.001
Si	0.041		

A typical microstructure of the specimen is shown in Fig. 5.1(a).

Experimental Conditions

It is necessary to achieve the steady-state condition in a reasonable time. Using DeGroot's method[35] (Chapter IV), suitable experimental conditions were determined as follows:

Table 5.2

Experimental Conditions

Specimen:	0.5 wt. % C steel (Cu plated)
Size:	O.D. 6mm; I.D. 3mm; length 1mm
Temperature:	927° C (1,200°K) measured by CA thermocouple
Atmosphere:	Vacuum, 10^{-5} to 10^{-6} torr
Time:	1, 8 and 24 hours
Heat Treatment after Electrotransport:[a]	Slow cooled (about 50°C/hr) from 750 to 650° C

[a]Slow cooling was used to facilitate later machining of the layers. This type of cooling also produced a microstructure, Fig. 5.1, that showed clearly the redistribution of carbon produced by electrotransport.

As shown in Table 5.2, the steel specimen was electroplated with copper to prevent loss of carbon during the experiment.

Preliminary Experimental Results

The microstructures of the steel specimen before and after electrotransport experiment, under the experimental conditions given

in Table 5.2, are shown in Fig. 5.1. The microstructures for 1-, 8- and 24-hour specimens demonstrate the migration of carbon towards cathode. Figure 5.2 is the microstructure of the steel specimen for the same kind of experiment as Fig. 5.1(c) (8 hours) except that the cooling rate is different. The microstructure of the rapidly-cooled specimen (the current was turned off abruptly after the experiment*) showed some evidence of the redistribution of carbon in the steel specimen caused by electrotransport. The carbon content may be expected to vary continuously from about 0.3 wt. % at the anode end to about 0.8 wt. % at the cathode end. The structure is a mixture of proeutectoid ferrite, fine pearlite and martensite. The slowly-cooled specimen, on the other hand, consisted of proeutectoid ferrite and pearlite.

The 8-hour specimen (slowly cooled) was sectioned using a lathe and was analyzed chemically** to obtain the curve shown in Fig. 5.3. It is clear that a redistribution of carbon has occurred. There is qualitative agreement with theory, but the quantitative discrepancies (the deviation at the anode end) were due to the slow cooling of the specimen and to the lack of accuracy of the chemical analysis.*** The results of Fig. 5.1 and Fig. 5.3, however, show that the steady-state can be attained in 8 hours, the time predicted theoretically, although these results do not represent the equilibrium at high temperature because of the effects of slow cooling.

*The temperature of the specimen decreased to less than 50 °C within 30 seconds after turning off the current.

**The chemical analysis of the specimen was done by the Armco Steel Corporation.

***Precision of the chemical analysis is $X \pm 0.02$~0.04 wt. %.

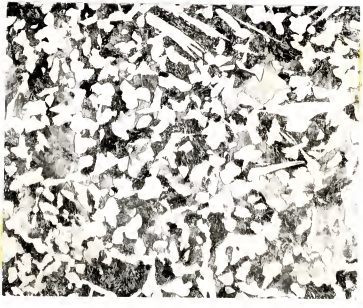

(a) Before electrotransport.

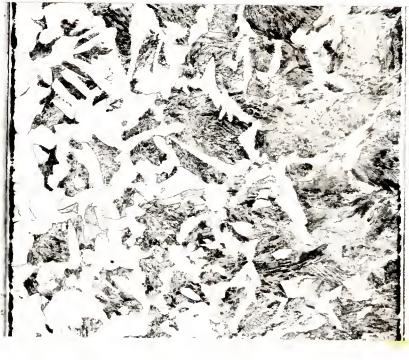

(b) After electrotransport for 1 hour.

Figure 5.1. Microstructures of 0.5% C steel before and after electrotransport at 927°C (slowly cooled). 100X

(c) After electrotransport for 8 hours.

(d) After electrotransport for 24 hours.

Figure 5.1. (Continued)

Figure 5.2. Microstructure of 0.5% C steel after electrotransport at 927° C (rapidly cooled). 100X

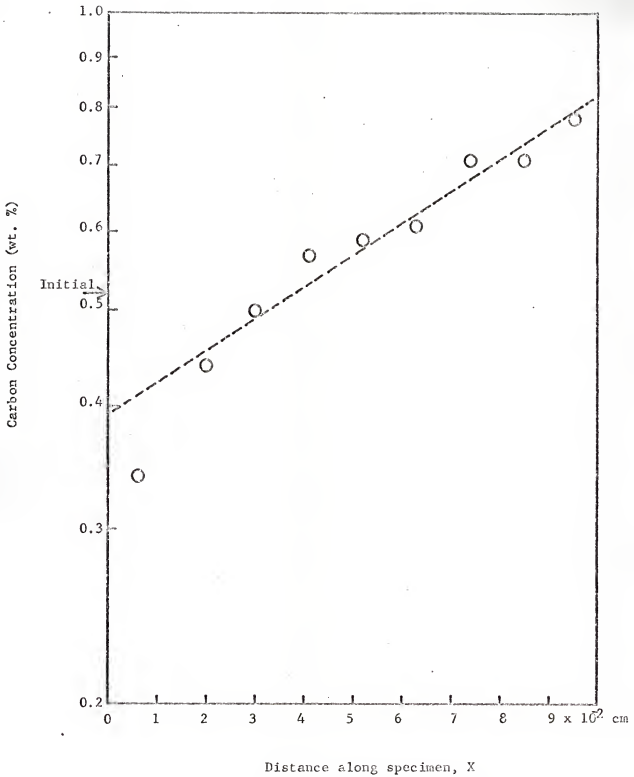

Figure 5.3. Carbon distribution after electrotransport (8 hours, 927°C), with copper plated specimen. The result was obtained by chemical analysis of carbon in the sectioned specimen.

Carbon Gain or Loss in the Specimen During the Experiment

As described in Chapter IV, an important requirement of the present experiment is to keep the carbon inside the specimen without any mass transfer between the external carbon source (graphite used to heat the specimen) or sink (vacuum atmosphere). This requirement was shown to be satisfied by comparing the carbon content of the specimen before and after electrotransport for 8 hours at 927°C.

Several electrotransport experiments were done with specimens cut from a single bar of the high-purity carbon steel shown in Table 5.1. Each specimen coated with copper and palladium was examined at two different vacuums ($\sim 10^{-4}$ and $\sim 10^{-6}$ torr). The carbon contents of the specimens subjected to electrotransport for 8 hours at 927°C are summarized in Table 5.3. The results show that the copper-coated specimens at higher vacuum atmosphere ($10^{-5} \sim 10^{-6}$ torr) satisfy the requirement, although some of the plated copper evaporated from the steel surface during the experiment. To correct this, palladium plating over the copper layer to decrease copper evaporation was suggested.

Table 5.3

The Carbon Content after Electrotransport

Specimen	Vacuum (torr)	Carbon Content[a] (wt. %)	Average
Initial	----	0.52	
(before experiment)	----	0.52	0.52
Cu plated	2×10^{-4}	0.75	
(10μ)	$1\times10^{-4} \sim 8\times10^{-5}$	0.62	0.69
Cu plated	1.5×10^{-5}	0.53	
(10μ)	$1.5\times10^{-5} \sim 6\times10^{-6}$	0.50	0.52
Pd plated	1×10^{-4}	0.77	
(5μ)	2×10^{-4}	0.55	0.66
Pd plated	2×10^{-6}	0.48	
(5μ)	5×10^{-6}	0.51	0.50
No coating	1×10^{-4}	0.55	0.55

[a]Carbon analyses were made using a Leco 50-Second Analyser at the Armco Steel Corporation. The accuracy expected is around $X \pm 0.02 \sim 0.03\%$.

CHAPTER VI

EXPERIMENTS WITH RADIOACTIVE CARBON, C^{14}

To obtain more precise data, radioactive carbon, C^{14}, was introduced into Armco iron as a tracer for the determination of the concentration profile after electrotransport. This procedure replaced the less accurate chemical method employed in the preliminary experiments.

Carburization

Carburization of Armco Iron

Radioactive carbon atoms were introduced to Armco iron (C 0.012, Mn 0.017, P 0.005, S 0.025 wt. %) through gas carburization with a mixture of charcoal carbon plus barium carbonate containing C^{14}, as $BaC^{14}O_3$. Transfer of carbon to the iron through the gas phase provided a desirable high specific activity.[37]

Table 6.1 gives the results of preliminary carburization of small Armco iron specimens (O.D. 6mm, I.D. 3mm and length 3mm) by a mixture of charcoal powder and $BaCO_3$ (not including C^{14}). In the carburization system, specimen and carburizing agent were kept separated in a copper container (Fig. 6.1), sealed in an evacuated Pyrex glass tube. The carbon content was evaluated metallographically.

Taking into consideration the preliminary experimental results, two groups of specimens, i.e., 0.1 and 0.5 wt. % carbon steels were made. In each carburization three specimens (each O.D. 6mm, I.D. 3mm

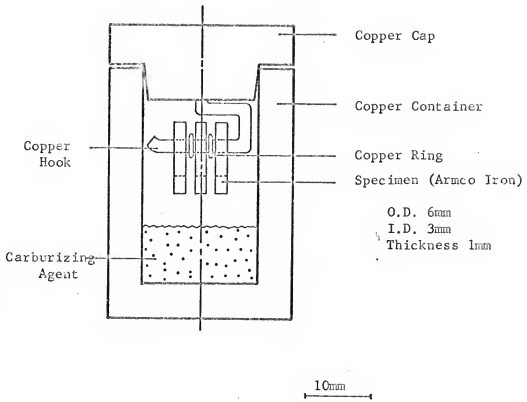

Figure 6.1. Carburization cell made of pure copper, shown with three 1mm thick specimens.

Table 6.1

Carbon Content Produced During
Preliminary Carburizing Studies

Temperature (°C)	Time (hrs.)	Carburizing Agent A	B	C	D
850	20			0.4	
875	20		< 0.1	0.4	
900	20	< 0.1	0.1	0.2	
950	20			0.3	0.4
975	20		0.2	0.5	
1,000	20			0.45	

A: Necessary amount for the carburization reaction to get 0.5% C steel:

$BaCO_3 + C + 3Fe \rightarrow BaO + Fe_3C + CO_2$

B: Theoretical amount, including carbon in gas phase.

C: B x 2

D: B x 3

and length 1mm*) were loaded into the copper vessel mentioned previously. The experimental conditions and the average carbon content of the specimen carburized are given in Table 6.2.

In each case about 0.4 mg of $BaC^{14}O_3$, whose activity is 0.26 ± 10% mc/mg (isotopic ratio is 84.2%), was added in a mixture of barium

*More precisely, specimens from 0.0418 inches (1,060μ) to 0.0425 inches (1,080μ) in length were prepared.

carbonate and charcoal powder. This is the amount necessary to obtain a specimen with a final beta activity of about 10^4 to 10^5 dpm.

Table 6.2

Conditions for Carburizing of Specimen Using C^{14}

Group	Expected Contents (wt. %)	$BaCO_3$ (g) C (g)	Temp. (°C)	Time (hr.)	Actual C Contents Average[a]
I	~ 0.5	0.880[b] 0.048	975	20	0.47±0.02
II	~ 0.1	0.220[c] 0.012	900	20	0.12±0.01

[a]Average of 7 different specimens.
[b]Theoretical amount (A) x 4.
[c]Theoretical amount (A) for the carburization reaction to get 0.5% C steel (carbon in gas phase is included)

Homogeneity of the Carburized Specimen

After carburizing, the homogeneity of the carbon in the specimen was determined by measuring the surface activity of a specimen. Each specimen was mounted in synthetic resin and was sectioned with a microtome.

Two typical results showing the homogeneity of the specimen are presented in Fig. 6.2. As shown in this figure, the concentration of carbon near the surface is very high compared to the homogeneous region deeper than 20-30μ below the surface of the specimen. This

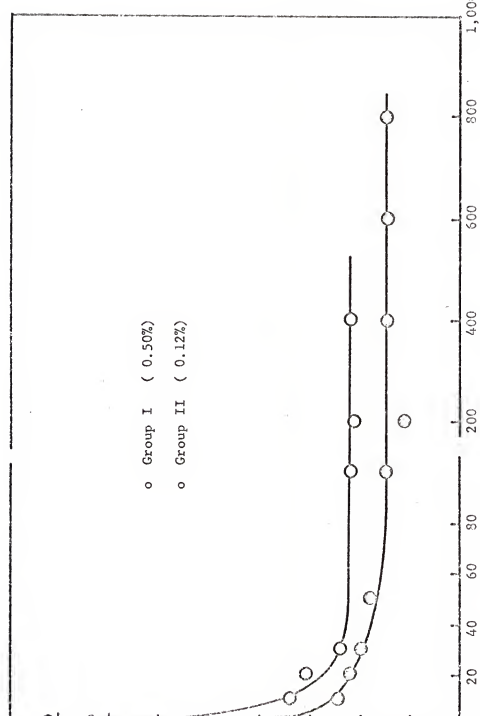

Figure 6.2. Typical distribution of carbon in two specimens after carburizing in a $BaCO_3$ + C mixture.

high-carbon region was studied more carefully by etching the surface of the specimen electrolytically. The result, Fig. 6.3, verified the phenomenon. This large amount of carbon near the surface may be considered as the result of the cementation from the CO-CO_2 mixture gas (more than 90% may be CO) during air-cooling after carburization. In practice, a homogeneous specimen can be obtained by removing a small surface layer. Electrolytic etching[38] (solution of H_2SO_4 250 cc/l and Na_2SO_4 125 g/l; temperature $<30°C$; cell voltage, 5V) was successfully used for this purpose.

The specimens were carburized in sets of three, as described above, to obtain three specimens with the same carbon content and activity. Two sets of specimens, which belonged to each group I (~0.5 wt. %) and II (~0.1 wt. %), are described in Table 6.3. Typical microstructures of the steel for each group are given in Fig. 6.4.

Surface Treatment of the Specimen

Preliminary experiments showed that carbon loss or addition to the specimen could be prevented by the combined use of a vacuum atmosphere (10^{-5} to 10^{-6} torr) and of a suitable coating on the specimen. A suitable coating procedure was to plate first with copper (~10μ) and then with palladium (~10μ) to prevent deterioration of the copper in the vacuum atmosphere. Carbon has a low solubility and a low rate of diffusion in copper,[39] so there was negligible loss of carbon provided the copper layer was present. Diffusion of both iron[40] and palladium[41] into the copper layer reduced its effectiveness after longer times of

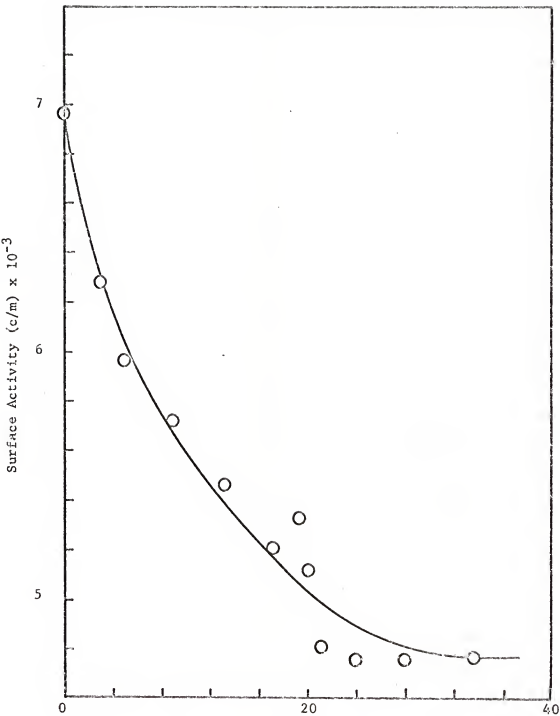

Figure 6.3. Carbon distribution at the vicinity of the surface.

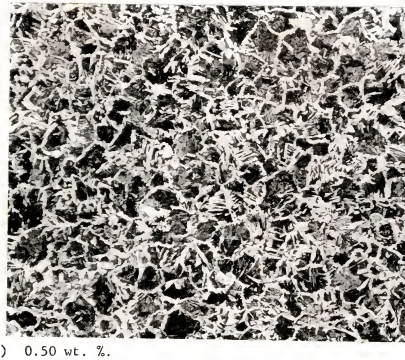

(a) 0.50 wt. %.

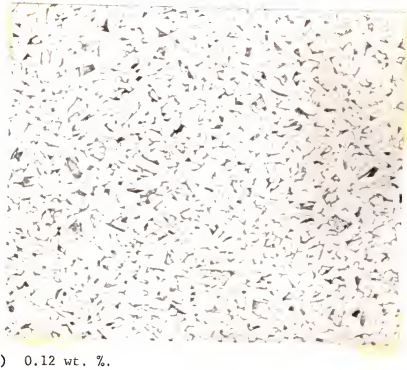

(b) 0.12 wt. %.

Figure 6.4. Typical microstructure of the specimen carburized with charcoal powder and barium carbonate containing C^{14}. 100X

Table 6.3

Carbon Content and Radioactivity
of the Carburized Specimen

Specimen		Carbon Content (wt. %)	Surface Activity (c/m)	Carburizing Condition		
				Carburizing Agent (g)	Temp. (°C)	Time (hr.)
Group I	A	0.12	7,100 7,200	C 0.012		
"	B	0.12	7,200 7,150	$BaCO_3$ 0.220	900	20
"	C	0.13	7,250 7,410			
Group II	A	0.47	10,200 10,600	C 0.048		
"	B	0.50	11,500 10,530	$BaCO_3$ 0.880	975	20
"	C	0.46	11,380 11,800			

electrotransport at 927° C (about 20 hours). Copper was plated from a cyanide bath and palladium from a high pH bath (for flash plating) and then from an acid palladium-chloride bath.

Carburized specimens were electrolytically polished to remove the high carbon region, to clean the surface itself and, further, to adjust the dimension of the thickness from 1,000 to 1,020μ. Next, copper and palladium electroplates, 10 to 12μ thick, were prepared using the electroplating conditions given in Table 6.4.

Table 6.4

Conditions for Copper and Palladium Electrolytic Plating[38]

Copper	Palladium
Copper Flash	First Coating[a] (1.5μ)
Solution: CuCN 15 g/l NaCN 23 g/l Na_2CO_3 15 g/l	Solution: Palladium RT (Technic Inc.)
Temperature: 50° C	pH: 5 ~ 7
Amp.: 10 mA (45 mA/cm^2)	Temperature: 25°C
Time: 2 min.	Amp.: 2.5 mA (12 mA/cm^2)
Cyanide Copper Bath	Time: 30 min.
Solution: CuCN 75 g/l NaCN 93 g/l NaOH 30 g/l	Anode: Stainless steel mesh
Temperature: 70 °C	Second Coating (10.5μ)
Amp.: 20 mA (91 mA/cm^2)	Solution: $PdCl_2$ 50 g NH_4Cl 13 g Water 1,000 ml HCl add to make 0.1 ~0.5 pH
Time: 18 min.	Temperature: 45 °C
	Amp.: 12 mA (55 mA/cm^2)
	Time: 25 min.
	Agitation: Mechanical
	Anode: Pure palladium

[a]To protect the copper layer from a corrosive acid chloride bath, a high pH palladium bath was employed.

Experimental Condition and Method of Electrotransport

The experimental procedures and the conditions of the electrotransport experiments are shown in Fig. 6.5 and Table 6.5, respectively.

One of the specimens, carburized in sets of three as described above, was analyzed radio-chemically without being subjected to electrotransport to furnish a comparison for the actual electrotransport specimens. Typically, a plated specimen, sandwiched between graphite discs, was placed in the specimen chamber, Fig. 3.2 (Chapter III). After the system was evacuated in the range 10^{-5} to 10^{-6} torr, the electric current was applied to the specimen. The length of the graphite discs determined the specimen temperature at a given value of current density. Discs 6mm long gave 927° C at a current density of 1,100 A/cm^2. Discs about 3.0 to 3.2mm long gave temperatures from 927° to 1,027° C at a current density of about 2,300 A/cm^2. A specimen was first heated to about 50°C below the desired temperature using manual control. When a potentiometer connected in parallel to the temperature-control system showed that the desired temperature had almost been reached, control was transferred to automatic operation. This initial heating required about five minutes. During the first hour or two of a run, the temperature-control system was watched carefully and the values of current were recorded. The temperature was controlled within $\pm$5°C. Because the graphite-steel-graphite sandwich was heated to a high temperature, the temperature gradient in the iron specimen in the direction of electrotransport was undetectably small. Observations with an optical pyrometer showed that it was less than 5°C over the 1mm length of the specimen.

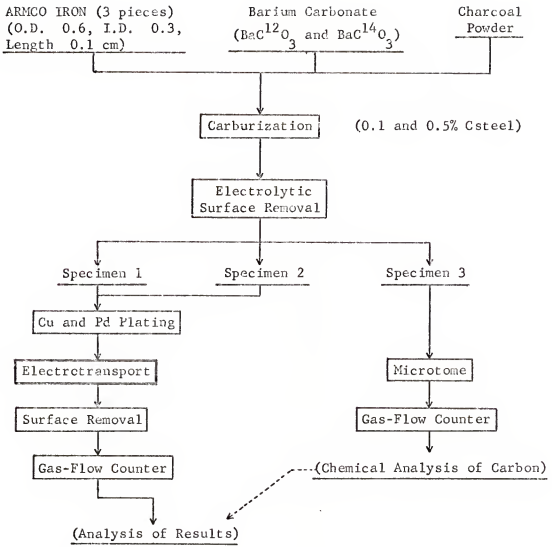

Figure 6.5. Experimental procedure for the electrotransport of carbon in γ iron, employing radioactive carbon, C^{14}.

Table 6.5

Experimental Condition for
Electrotransport of C^{14} in Iron

Specimens:	0.12 and 0.47 wt. % (average) C steel Coated with Cu and Pd
Size:	O.D. 6mm; I.D. 3mm; Length 1mm
Temperatures:	927°, 977° and 1,027°C
Atmosphere:	Vacuum, $10^{-5} \sim 10^{-6}$ torr
Current Density:	About 2,600 and 1,100 (only for 927°C) A/cm^2
Times:	15 min. to 24 hours
Cooling rate after experiment:	Rapid cooling[a]

[a]The temperature of the specimen decreased to less than 50°C within 30 seconds after turning off the current.

About 2mm of each graphite disc was at red heat with a current density of 2,300 A/cm^2 and 3mm with 1,100 A/cm^2. The vacuum reading increased to 10^{-4} torr during initial heating, but returned to the 10^{-5} to 10^{-6} torr range within 1 minute. To terminate a run, the system was transferred to manual control and the current was turned off. The specimen then cooled to less than 50°C within 30 seconds.

After electrotransport the specimens were clean and bright and showed no deterioration. Usually the specimen could be separated easily from the graphite discs, but sometimes the graphite was removed by grinding to avoid possible damage to the specimen. No radioactive carbon could be detected in the graphite.

The treated specimen was mounted in a synthetic resin (8.5 g) and the surface radioactivity of the specimen was measured. Usually this activity was only about 1% that of the main portion of the specimen. In a pair of comparable specimens, one was mounted to expose the anodic surface and the other to expose the cathodic surface.

Gas-flow detector, Model 480, and manual scalor, Model 8775 (Nuclear Chicago Corporation), were used to count the beta rays emitted from the specimen. Each specimen, mounted in the synthetic resin, was placed under an end-window detector. The geometrical arrangement for measuring is given in Appendix II. Hand polishing with a belt surfacer and a hand grinder (grits No. 240 to 600) and also sectioning with a microtome were successfully used to remove successive layers of thickness from about 10 to 150 microns. Since the range, R, of beta rays of C^{14} and the corresponding thickness of iron are R = 20 mg/cm^2 and 25 microns,[42] it is possible to evaluate the disintegration of a radioactive carbon at, for example, each successive layer of about 100 microns provided $\mu(\ell)$ is constant,[43] where $\mu(\ell)$ is the linear absorption coefficient. The thickness of each layer removed was measured with a micrometer, and then thin flat glass plates (100 and 200μ thickness) were inserted under the specimen holder (see Appendix II)to compensate for the increase in distance between the surface of the resin and the window of the detector. Preset counts of 10^4 were used, since the radioactivity of the specimen is high enough (2,000 ~ 10,000 c/m) for this kind of detection. The performance of the detector was verified using a standard sample (C^{14}; 0.1μc) every half-hour or so during the measurement. The accuracy was $\pm$1% for 10^4 preset counts. Background

measurements were made periodically during the counting procedure and ranged from 25 to 31 c/m.

The third specimen in each set of three carburized specimens was mounted in a synthetic resin without plating after removing a small region of the surface by electrolytic etching. First, about 200μ of the surface was removed by microtoming and the surface radioactivity was measured. Next, the mounting material was removed from the specimen, using acetone and the specimen was subjected to ordinary chemical carbon analysis. This procedure established the relation between the radioactivity and the carbon content for the three specimens carburized together.

The experimental data were plotted as radioactivity* vs. distance curves. On the assumption of no carbon loss or addition to the specimen during the experiment (discussed above), the radioactivity values were converted to carbon content by the method described in Appendix III. For this conversion, diffusion in the plated layer is also considered. The penetration of the plated copper and palladium into the steel specimen after electrotransport was measured using an optical microscope. Electron microprobe analysis verified the extent of this diffusion phenomenon. The penetration was found to be about 15μ. To determine the value of the apparent charge, Z*, S was determined from the semi-log plot of carbon content vs. distance.

*Since the value of the background was very low compared to the radioactivity of the specimen and was stable as described above, the background value was not used[44] to draw the graph.

Results of the Electrotransport Experiment

Cooling Rate of the Specimen After the Electrotransport

One of the reasons for discrepancies between the theoretical curve and the experimental curve in the specimen analyzed chemically was the cooling rate of the specimen as described in Chapter V.

Figure 6.6 is the semi-log plot of the carbon radioactivity of the specimen vs. the distance along the specimen cooled slowly (cooled about 50°C/hr from 750° to 650°C) and cooled rapidly (cooled to less than 50°C within 30 seconds after the experiments). All experiments were done at 927°C for 8 hours with 0.47% carbon steel coated with Cu-Pd layer. The plot for the rapidly cooled specimen fits the straight line which proves the attainment of the steady-state, while slowly cooled specimens show a deviation from a straight line at the anode end. The same phenomenon, i.e., the depletion of the carbon content at the anode end, was observed in the specimen analyzed chemically as is shown in Fig. 5.3 (Chapter V). On the other hand, the deviation was not found at the cathode end (Fig. 6.6).

The above results show that it is necessary to cool the specimen very rapidly after the experiment, in order to retain the steady-state condition at room temperature.

Confirmation of Attainment of the Steady-State

The results of electrotransport at 927°C for times in the range of 15 minutes to 24 hours are shown in Fig. 6.7 for a 0.47% carbon steel. The semi-log plots for the same data (for 8 and 24 hour experiments) are shown in Fig. 6.8. The results of these measurements are

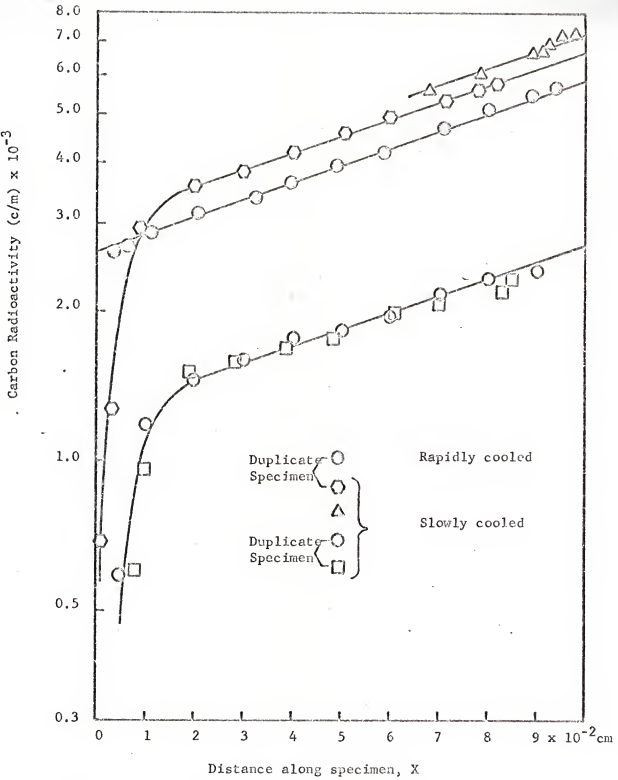

Figure 6.6. The carbon-activity vs. distance along the specimen. Comparison of the rapidly and slowly cooled specimen obtained from the experiment for 8 hours at 927°C with about 2,200 A/cm^2 in 0.47% carbon steel.

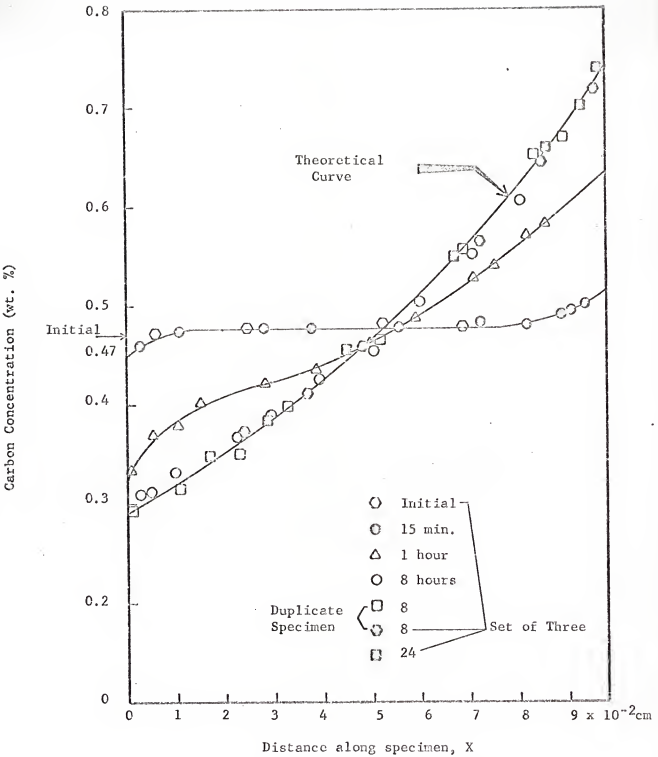

Figure 6.7. Carbon distribution after electrotransport for 15 minutes to 24 hours at 927°C with 2,170 A/cm^2 in a 0.47 wt. % carbon steel.

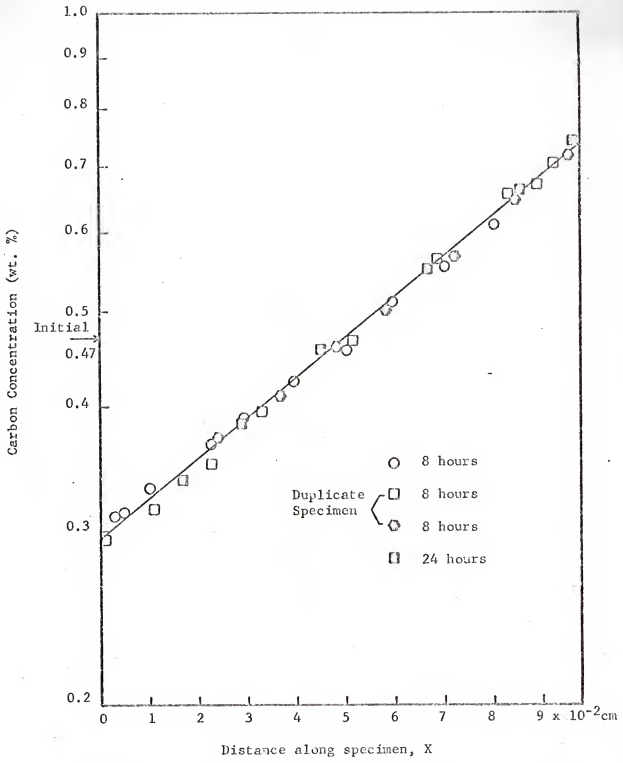

Figure 5.8. Semi-log plots of carbon concentration vs. distance along the specimen after electrotransport for 8 to 24 hours at 927°C with 2,170 A/cm^2 in 0.47 wt. % carbon steel.

given in Tables 6.6 to 6.11. The process of redistribution of carbon occurs in the manner predicted by theory, as described above. In particular, the steady-state curve, Eq. (4.16), with n_{min} = 0.295 and n_{max} = 0.740 wt. % carbon coincided with the data points from both 8-hour and 24-hour experiments. It can be concluded that the steady-state condition was attained in the 8-hour period predicted theoretically, Eq. (4.12).

The "initial" specimen in Fig. 6.7 was carburized simultaneously with two 8-hour specimens, but it was not subjected to electrotransport. If a negligible amount of carbon was either added to or lost from the specimens during electrotransport, then the area under the curve for an 8-hour specimen should be the same as that under the initial specimen. This condition is fulfilled within experimental error, as was proved by the chemical analysis of the specimen after electrotransport (Chapter V), and justifies the analysis of the data, assuming a stationary state of the carbon concentration.

Value of the Apparent Charge, Z*

The results of the experiments for two carbon levels, three temperatures, and various current densities are given in Tables 6.12 to 6.24. The semi-log plots of these data (and the duplicated specimens as well) are given in Figs. 6.9 to 6.15.

The value of S, Eq. (A 1.7), was evaluated for the electrotransport experiment corresponding to the above different experimental conditions, Table 6.25. From Eq. (4.15), the apparent charge, Z*, was then calculated. The necessary data on the resistivity of iron were

obtained from the 1948 ASM Metals Handbook. The value of Z* is $+3.9_5 \pm 0.0_8$, close to the normal +4 valence of carbon.

Table 6.6

Surface Activity Measurements

Sample: 52-B
Carbon Content: 0.47 wt. %
Condition: 927°C; 15 minutes; 1.65×10^3 A/cm^2; 5×10^{-5} torr

Surface Activity Data

Distance (μ)	Sample Activity (c/m)	Carbon Content (wt. %)
40	4,030	0.500
71	4,000	0.496
109	3,970	0.492
173	3,870	0.480
254	3,930	0.487
417	3,840	0.477
600	3,840	0.477
695	3,860	0.478
870	3,860	0.478
950	3,705	0.459

Table 6.7

Surface Activity Measurements

Sample: 54-A
Carbon Content: 0.47 wt. %
Condition: 927° C; 1 hour; 2.24×10^3 A/cm^2; 5×10^{-4} torr

Surface Activity Data

Distance (μ)	Sample Activity (c/m)	Carbon Content (wt. %)
10	2,480	0.333
56	2,750	0.369
104	2,820	0.378
152	2,940	0.394
284	3,120	0.418
389	3,250	0.433
501	3,420	0.458
593	3,680	0.468
713	3,940	0.528
754	4,020	0.539
813	4,250	0.570
854	4,530	0.583

Table 6.8

Surface Activity Measurements

Sample: 52-A
Carbon Content: 0.47 wt. %
Condition: 927°C; 8 hours; 2.15 x 10^3 A/cm^2; 8 x 10^{-6} torr

Surface Activity Data

Distance (μ)	Sample Activity (c/m)	Carbon Content (wt. %)
28	2,600	0.310
53	2,640	0.313
101	2,840	0.332
223	3,080	0.367
294	3,270	0.390
394	3,560	0.425
503	3,820	0.455
600	4,275	0.510
704	4,630	0.552
803	5,025	0.610

Table 6.9

Surface Activity Measurements

Sample: 53-A
Carbon Content: 0.47 wt. %
Condition: 927° C; 8 hours; 2.31×10^3 A/cm^2; 5×10^{-5} torr

Surface Activity Data

Distance (μ)	Sample Activity (c/m)	Carbon Content (wt. %)
10	2,800	0.290
107	2,780	0.315
224	3,050	0.345
328	3,820	0.394
514	4,110	0.465
692	5,460	0.562
844	6,300	0.649
895	6,450	0.664

Table 6.10

Surface Activity Measurements

Sample: 53-B
Carbon Content: 0.47 wt. %
Condition: 927°C; 8 hours; 2.19 x 10^3 A/cm^2; 4 x 10^{-5} torr

Surface Activity Data

Distance (μ)	Sample Activity (c/m)	Carbon Content (wt. %)
20	6,950	0.716
129	6,400	0.645
256	5,540	0.566
396	4,890	0.500
496	4,410	0.454
611	3,985	0.410
750	3,640	0.370

Table 6.11

Surface Activity Measurements

Sample: 59-A
Carbon Content: 0.47 wt. %
Condition: 927° C; 24 hours; 2.26×10^3 A/cm^2; 4×10^{-5} torr

Surface Activity Data

Distance (μ)	Sample Activity (c/m)	Carbon Content (wt. %)
15	6,675	0.737
56	6,390	0.705
119	5,975	0.660
307	5,100	0.553
531	4,150	0.458
690	3,500	0.386
812	3,050	0.337

Table 6.12

Surface Activity Measurements

Sample: 9-B
Carbon Content: 0.50 wt. %
Condition: 977° C; 5 hours; 2.51 x 10^3 A/cm^2; 2 x 10^{-5} torr

Surface Activity Data

Distance (μ)	Surface Activity (c/m)	Carbon Content (wt. %)
30	10,650	0.770
83	10,300	0.726
177	9,350	0.659
347	8,000	0.564
492	7,000	0.494
629	5,880	0.415
764	5,200	0.367

Table 6.13

Surface Activity Measurements

Sample: 56-C
Carbon Content: 0.47 wt. %
Condition: 1,027°C; 3 hours; 2.31×10^3 A/cm^2; 3×10^{-5} torr

Surface Activity Data

Distance (μ)	Surface Activity (c/m)	Carbon Content (wt. %)
10	1,085	0.275
43	1,140	0.281
96	1,260	0.310
225	1,580	0.360
403	1,800	0.442
497	2,000	0.485
606	2,190	0.517
708	2,360	0.601

Table 6.14

Surface Activity Measurements

Sample: 56-B
Carbon Content: 0.47 wt. %
Condition: 1,027°C; 3 hours; 2.83×10^3 A/cm^2; 3×10^{-5} torr

Surface Activity Data

Distance (μ)	Surface Activity (c/m)	Carbon Content (wt. %)
20	2,940	0.771
61	2,930	0.736
142	2,675	0.659
330	2,155	0.553
510	1,770	0.454
647	1,560	0.400
774	1,310	0.366

Table 6.15

Surface Activity Measurements

Sample: 57-C
Carbon Content: 0.47 wt. %
Condition: 927°C; 8 hours; 1.35×10^3 A/cm^2; 2×10^{-5} torr

Surface Activity Data

Distance (μ)	Surface Activity (c/m)	Carbon Content (wt. %)
20	1,375	0.343
101	1,450	0.361
203	1,570	0.392
381	1,740	0.435
480	1,850	0.461
595	1,970	0.492
704	2,140	0.535
811	2,330	0.582

Table 6.16

Surface Activity Measurements

Sample: 59-B
Carbon Content: 0.47 wt. %
Condition: 927°C; 8 hours; 1.43×10^3 A/cm^2; 3×10^{-5} torr

Surface Activity Data

Distance (μ)	Surface Activity (c/m)	Carbon Content (wt. %)
15	6,100	0.633
162	5,620	0.583
276	5,130	0.532
398	4,760	0.494
619	4,100	0.426
751	3,880	0.402

Table 6.17

Surface Activity Measurements

Sample: 15-A
Carbon Content: 0.12 wt. %
Condition: 927° C; 12 hours; 2.46 x 10^3 A/cm^2; 3 x 10^{-5} torr

Surface Activity Data

Distance (μ)	Surface Activity (c/m)	Carbon Content (wt. %)
20	3,540	0.186
124	4,170	0.172
275	3,695	0.153
389	3,270	0.134
635	2,500	0.108
747	2,300	0.098
860	2,140	0.091

Table 6.18

Surface Activity Measurements

Sample: 11-B
Carbon Content: 0.14 wt. %
Condition: 927° C; 12 hours; 1.98×10^3 A/cm^2; 2×10^{-5} torr

Surface Activity Data

Distance (μ)	Surface Activity (c/m)	Carbon Content (wt. %)
20	1,885	0.085
230	2,620	0.104
309	2,885	0.115
423	3,310	0.132
504	3,595	0.143
606	4,000	0.160
710	4,460	0.178
812	5,020	0.200

Table 6.19

Surface Activity Measurements

Sample: 13-A
Carbon Content: 0.13 wt. %
Condition: 977°C; 6 hours; 2.26 x 10^3 A/cm^2; 3 x 10^{-5} torr

Surface Activity Data

Distance (μ)	Surface Activity (c/m)	Carbon Content (wt. %)
31	4,020	0.207
102	3,780	0.196
211	3,425	0.177
303	3,130	0.161
407	2,900	0.146
534	2,600	0.135
656	2,180	0.112
758	2,000	0.105
837	1,800	0.098

Table 6.20

Surface Activity Measurements

Sample: 13-B
Carbon Content: 0.13 wt. %
Condition: 977° C; 6 hours; 2.12 x 10^3 A/cm^2; 3 x 10^{-5} torr

Surface Activity Data

Distance (μ)	Surface Activity (c/m)	Carbon Content (wt. %)
26	1,930	0.090
143	2,205	0.102
331	2,540	0.117
486	2,915	0.135
644	3,175	0.147
801	3,600	0.177

Table 6.21

Surface Activity Measurements

Sample: 14-A
Carbon Content: 0.11 wt. %
Condition: 1,027°C; 3.5 hours; 2.22 x 10^3 A/cm^2; 2 x 10^{-5} torr

Surface Activity Data

Distance (μ)	Surface Activity (c/m)	Carbon Content (wt. %)
30	1,625	0.072
145	1,920	0.081
280	2,120	0.095
399	2,340	0.104
526	2,660	0.117
628	2,840	0.125
740	3,020	0.135
832	3,220	0.153

Table 6.22

Surface Activity Measurements

Sample: 14-B
Carbon Content: 0.11 wt. %
Condition: 1,027°C; 3.5 hours; 2.40 x 10^3 A/cm^2; 4 x 10^{-5} torr

Surface Activity Data

Distance (μ)	Surface Activity (c/m)	Carbon Content (wt. %)
30	4,200	0.178
111	3,970	0.168
250	3,340	0.141
431	2,810	0.119
550	2,440	0.103
690	2,100	0.089

Table 6.23

Surface Activity Measurements

Sample: 12-B
Carbon Content: 0.12 wt. %
Condition: 927°C; 12 hours; 1.10×10^3 A/cm^2; 1×10^{-5} torr

Surface Activity Data

Distance (μ)	Surface Activity (c/m)	Carbon Content (wt. %)
10	4,600	0.097
119	4,950	0.102
203	5,150	0.105
325	5,510	0.112
500	6,020	0.123
599	6,330	0.129
718	6,800	0.137
827	6,950	0.145

Table 6.24

Surface Activity Measurements

Sample: 60-A
Carbon Content: 0.12 wt. %
Condition: 927°C; 12 hours; 1.49 x 10^3 A/cm^2; 4 x 10^{-5} torr

Surface Activity Data

Distance (μ)	Surface Activity (c/m)	Carbon Content (wt. %)
30	3,375	0.171
233	2,990	0.148
385	2,620	0.134
545	2,350	0.119
647	2,130	0.108
770	2,035	0.103

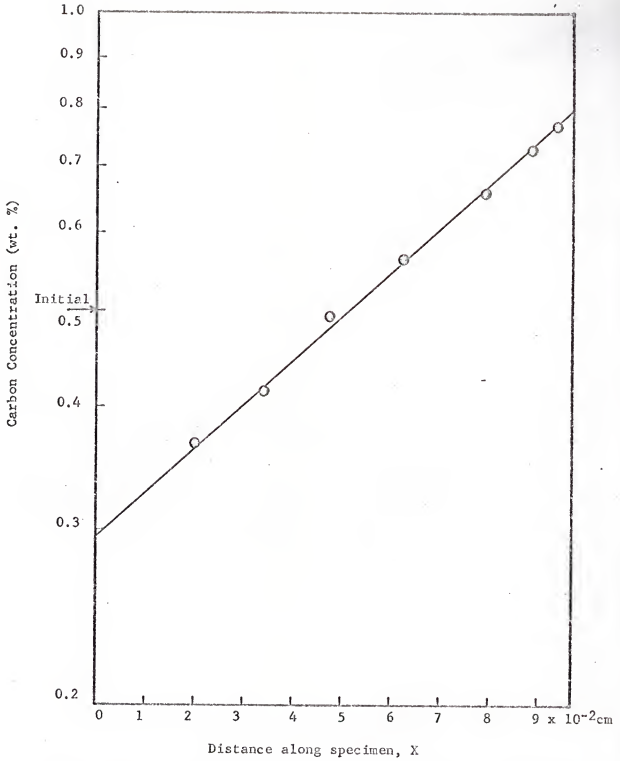

Figure 6.9. Semi-log plots of carbon concentration vs. distance along the specimen after electrotransport for 5 hours at 927°C with 2,570 A/cm^2 (0.50 wt. % carbon steel).

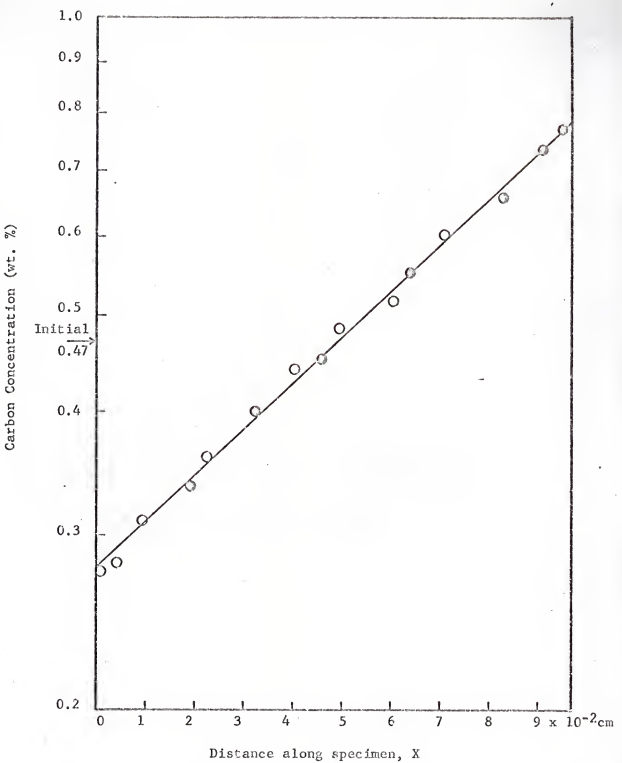

Figure 6.10. Semi-log plots of carbon concentration vs. distance along the specimen after electrotransport for 3 hours at 1,027°C with 2,570 A/cm^2 (0.47 wt. % carbon steel).

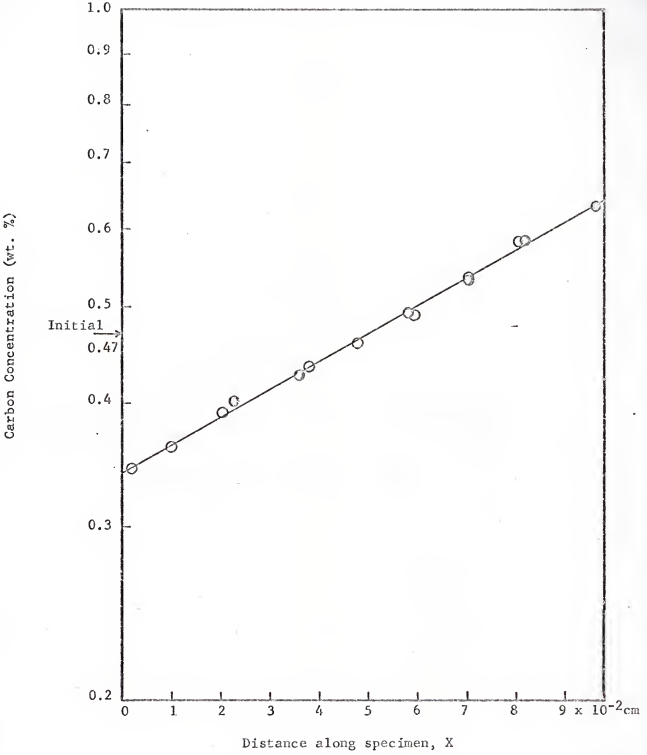

Figure 6.11. Semi-log plots of carbon concentration vs. distance along the specimen after electrotransport for 8 hours at 927°C with 1,390 A/cm^2 (0.47 wt. % carbon steel).

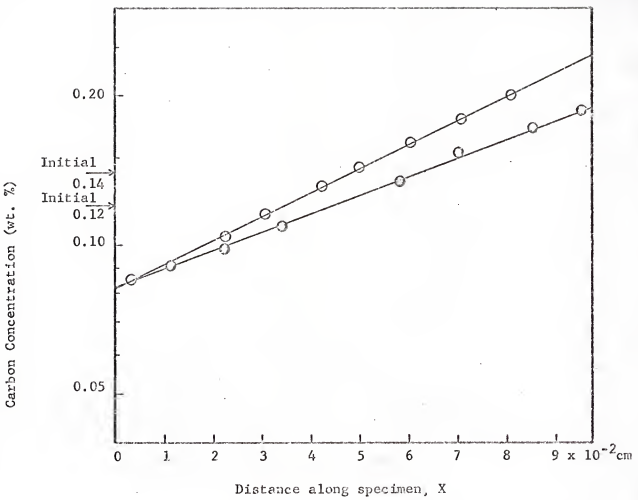

Figure 6.12. Semi-log plots of carbon concentration vs. distance along the specimen after electrotransport for 12 hours at 927°C with 2,460 and 1,980 A/cm^2 (0.12 and 0.14 wt. % carbon steel).

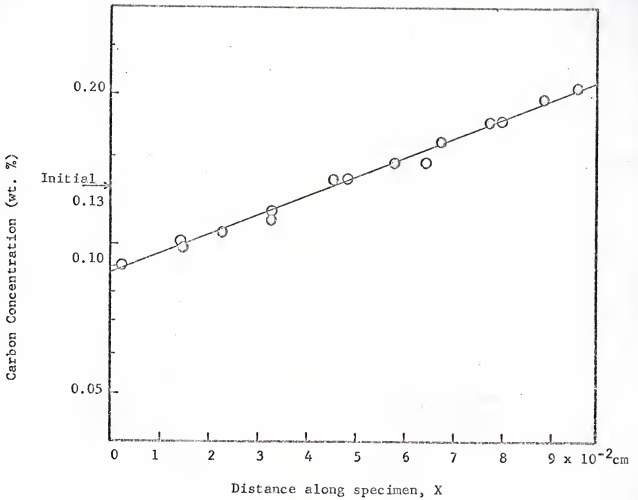

Figure 6.13. Semi-log plots of carbon concentration vs. distance along the specimen after electrotransport for 6 hours at 927°C with 2,190 A/cm^2 (0.13 wt. % carbon steel).

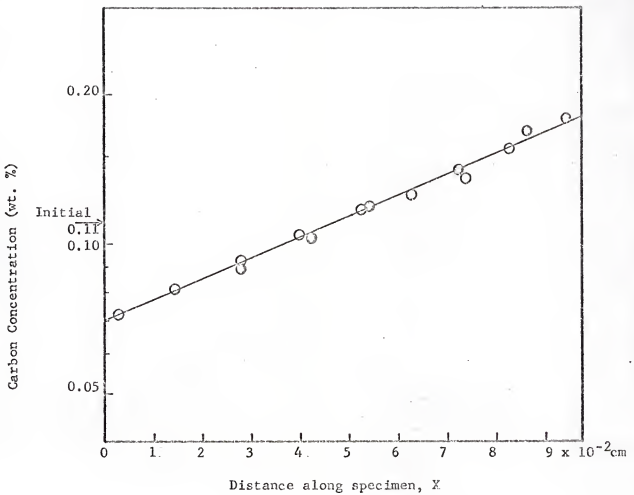

Figure 6.14. Semi-log plots of carbon concentration vs. distance along the specimen after electrotransport for 3.5 hours at 1,027°C with 2,330 A/cm^2 (0.11 wt. % carbon steel).

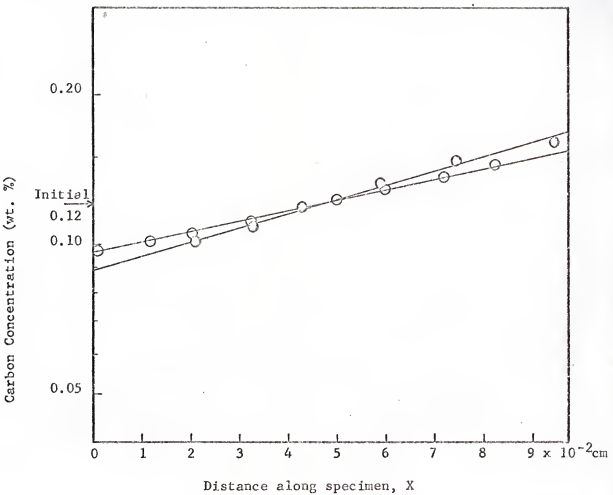

Figure 6.15. Semi-log plots of carbon concentration vs. distance along the specimen after electrotransport for 12 hours at 927°C with 1,100 and 1,490 A/cm^2 (0.12 wt. % carbon steel).

Table 6.25

The Apparent Charge, Z*,
of Carbon in γ Iron

Sample Number	Specimen Carbon Content (wt. %)	Length of Initial Specimen (μ)	Thickness of Diffusion + Plated Layer[a] (μ)	Thickness of the Steel after the Experiment (μ)
52-A	0.47	998	35	978
53-B	0.47	1,002	35	982
9-B	0.50	1,000	41	968
56-C	0.47	1,010	43	974
56-B	0.47	1,005	43	969
57-C	0.47	1,001	35	981
59-B	0.47	999	35	979
15-A	0.14	1,010	42	976
11-B	0.12	1,010	42	976
13-A	0.13	1,018	41	986
13-B	0.13	1,022	41	990
14-A	0.11	1.006	43	970
14-B	0.11	1,014	43	978
12-B	0.12	1,008	42	974
60-A	0.12	1,012	42	978

[a]Initial plated layer was estimated to be 25μ (Cu 12.5 and Pd 12.5μ) from the measurement of the weight increase during the copper and palladium plating.

Table 6.25 (Extended)

Temperature (°C)	Time (hr.)	Vacuum (torr)	Mean Current Density (A/cm^2)	n_{min} (wt. %)	n_{max} (wt. %)	S	Z*	Z* Average
927	8	$8x10^{-6}$	$2.15x10^3$	0.295	0.740	0.92	+3.9	
927	8	$4x10^{-5}$	2.19	0.295	0.740	0.92	+3.9	+3.9
977	5	$2x10^{-5}$	2.51	0.295	0.800	1.00	+3.8	+3.8
1,027	3	3	2.31	0.280	0.790	1.04	+3.9	
1,027	3	3	2.83	0.280	0.790	1.04	+3.9	+3.9
927	8	2	1.35	0.342	0.642	0.63	+4.1	
927	8	3	1.43	0.342	0.642	0.63	+4.1	+4.1
927	12	3	2.46	0.081	0.240	1.09	+3.9	
927	12	2	1.98	0.082	0.190	0.84	+4.1	+4.0
977	6	3	2.26	0.087	0.212	0.89	+3.9	
977	6	3	2.12	0.087	0.212	0.89	+3.9	+3.9
1,027	3.5	2	2.22	0.070	0.180	0.94	+4.0	
1,027	3.5	4	2.40	0.070	0.180	0.94	+4.0	+4.0
927	12	1	1.10	0.097	0.155	0.47	+4.0	
927	12	4	1.49	0.089	0.170	0.65	+3.9	+4.0

CHAPTER VII

DISCUSSION AND CONCLUSIONS

Diffusion Between Steel and Electroplated Layers

It was found that the plated layers, copper and palladium, diffused into each other and into the steel specimen. The results of electron microprobe analyses showed that copper and iron tend to diffuse outward, while palladium diffuses towards the inside of the specimen during the course of the experiment. Although about 15μ penetration of copper and palladium into the steel specimen was observed, this distance is comparatively small compared to the specimen thickness, 1,000μ. Since the qualitative estimates of carbon radioactivity in this diffusion layer indicated low values (usually the radioactivity in the diffusion layer was less than 5% of that at the steel surface), this diffusion layer had a negligible influence on the results.

Experimental Errors

The usual statistical analysis of the entire set of data on Z* gave a value of $+3.9_5 \pm 0.0_8$ at the 95% confidence level. In an effort to compare this $\pm 0.0_8$ value of precision with the actual conditions of the experiment, the following possible sources of error were considered:

(1) Attainment of steady-state condition.

(2) Measurement of the length of the specimen during surface removal.

(3) Measurements of temperature and current.

(4) Counting of radioactivity.

(5) Conversion from the curve of carbon activity vs. distance to the curve of carbon concentration vs. distance.

(6) Extrapolation of the curve of carbon concentration vs. distance to obtain the experimental parameter, S.

Evidence such as the straight-line plots of the log (concentration) vs. distance curves shows that the steady-state condition was closely approached. Also, in view of the type of variation in the curve of concentration vs. distance as the steady-state is approached, Fig. 6.7, the estimated 1% departure from the steady-state would cause only a fraction of 1% error in the value of Z*. A value of about -0.5% systematic error has been estimated.

Errors in the measurement of distance were of two types. The copper-palladium plated layer needed to be removed, together with about 15μ of the steel specimen into which the plated layer had diffused. This surface layer was removed by careful grinding with a belt surfacer and a hand grinder. Three percent nital solution was used to detect the presence of the steel surface as it became exposed. It was estimated that about $\pm$ 10μ error might have been made in locating the position of the steel surface after the removal of the diffused layer. This factor has little effect on the value of S because S is computed as the ratio of n_{max} and n_{min}.

The distance at which each of the radioactive counts was made was determined by a micrometer with an accuracy of about $\pm$ 2.5μ. This uncertainty is also expected in the measurement of the length and

diameter of the specimen. Although each specimen was tilted by some small, random amount from perfect parallelism when it was mounted in the synthetic resin, and also may have been uneven during the grinding, these two factors have little effect on the value of S for the following reason. The value of S was the average of duplicate specimens in which the measurements were made from the cathode end in one case and from the anode end in the other. The effect of tilt and uneven grinding would act in opposite directions in the two specimens and so the error would tend to be eliminated during averaging.

As described above, the fluctuation of the temperature of the specimen was $\pm$ 5°C. The standard deviation in the temperature may be estimated to be about 2.5°C, assuming that $\pm$ 5°C is the 95% confidence limit. The systematic error in the temperature can be neglected since the chromel-alumel thermocouple was calibrated with a standard Pt-Pt·Rh thermocouple. Some error also occurs in the measurement of the current through the specimen. Since the uncertainty in reading the current was $\pm$ 5 amperes, the standard deviation is about 2.5 amperes. The corresponding fractional standard deviation is, for example, about 0.5% for the experiment at 977°C with 2,500 A/cm^2.

Since 10^4 preset counts were used, the standard deviation for the counting rate, σ_R, is given by,[45]

$$\sigma_R = \sqrt{N}/t \tag{7.1}$$

where N is the total counts and t is the time of counting. Therefore, $\sigma_R = \frac{\sqrt{10,000}}{3.3} \simeq 30$ c/m. This is 1% of the fractional standard deviation since a typical activity was 3,000 c/m. This gives about $\pm$ 2% error

for the 95% confidence limit. Since $\pm$ 1% error is expected from the performance of the apparatus, the total error for each measurement is $\pm \sqrt{2^2+1^2} = \pm$ 2.2% by the law of addition of independent errors.[46] An average of seven measurements was made for one specimen. Therefore, the 95% confidence limit for the fluctuation in the linear plots can be estimated as $\pm 2.2/\sqrt{7} \simeq \pm$ 0.8%. Consequently, the fractional standard deviation is about 0.4%, and the standard deviation of $S \left(= \ln \frac{n_{max}}{n_{min}}\right)$ of the measurements of radioactivity can be calculated to be $\sqrt{(0.4)^2+(0.4)^2} = 0.57$, since the standard deviation of the natural logarithm of X is equal to the fractional standard deviation of X.[47] Since the value of S is, for example, about 1 for the case of the experiment mentioned above, the standard deviation equals the fractional standard deviation.

The conversion from curves of carbon-activity vs. distance to curves of carbon-concentration vs. distance is expected to cause negligible error. Even if the chemical determination of carbon content were somewhat in error, the corresponding error in Z* is negligible, since S is evaluated from the ratio of n_{max} and n_{min} and not from a single value.

The straight-line plots of carbon content vs. distance could be made quite accurately, thus giving values of n_{max} and n_{min} is of good precision. The error in n_{max} and n_{min} from this source was estimated to be $\pm$ 1.0% at most. Thus, the combined fractional standard deviation of S is $\sqrt{(0.57)^2+(0.5)^2} = 0.76\%$.

Finally, the fact that radioactivity came from a layer of finite thickness below the surface was neglected in plotting the data. However,

this contribution to the error is similar to the case of the inclination of the specimen during surface removal and can be neglected since duplicate specimens were used.

Now, the following relation, which was rewritten from Eq. (4.15), is useful for evaluating the combined errors for Z*;

$$Z^* = \frac{SkT}{\rho \ell e (I/A)} \tag{7.2}$$

where I is the current and A is the cross-sectional area of the specimen. Since the fractional standard deviation of a product or quotient is equal to the square root of the sum of the squares of the fractional standard deviations of the measured quantities,[47] the combined fractional standard deviation of Z*, σ'_{Z^*}, caused by the above random errors is

$$\begin{aligned} \sigma'_{Z^*} &= \sqrt{(\sigma'_I)^2+(\sigma'_A)^2+(\sigma'_T)^2+(\sigma'_\ell)^2+(\sigma'_S)^2} \\ &= \sqrt{(0.5)^2+(0.14)^2+(0.25)^2+(0.13)^2+(0.76)^2} \\ &= 0.965\% \end{aligned} \tag{7.3}$$

In Eq. (7.3) σ'_I, σ'_A, σ'_T, σ'_ℓ, and σ'_S are the fractional standard deviations for the terms with the corresponding suffixes. Multiplying σ'_{Z^*} by 1.96 gives the fractional error of Z* within the 95% confidence limit as $\pm$ 1.89%. This corresponds to $\pm$ 0.075 in the units of Z*. The value of Z* is, therefore, $3.9_5 \pm 0.0_8$, using the average of the experimental and statistical errors.

The systematic errors must be considered also. The measurement of the initial length of the specimen was made using a flat-tip micrometer. Consequently, the measured value represents the maximum height

if the specimen had non-parallel faces. Test measurements on five specimens showed that the average difference in height is about 10μ. Thus, the actual effective length for an average specimen was about 5μ less than the measured value. The length of the specimen, "ℓ", enters in the denominator in the calculation of Z*, Eq. (4.15). Therefore, the systematic error in length of the specimen increases the value of Z* by about -0.8%. Considering also the other systematic error, the deviation from the steady-state condition described above, the total systematic error in Z* is about -1.0%. Thus, the average experimental value of Z*, $+3.9_5 \pm 0.0_8$, should be corrected to $+3.9_9 \pm 0.0_8$ or more simply to 4.0 ± 0.1.

Significance of the Investigation

As discussed previously, one of the advantages of the steady-state method is the fact that it is unnecessary to use the chemical diffusion coefficient in calculating the effective charge. For this reason the present method may give unusually precise values for the apparent charge, provided the other experimental errors are small. Also, the experimental method and measurements are simple compared to those for the unsteady-state method. The effective charge of carbon in γ iron, $+3.9_9 \pm 0.0_8$, obtained in the present experiment can be considered especially reliable.

Three explanations of these results might be given.

(1) The force exerted on the migrating carbon ion is due only to the electrostatic force of the field, E, on the charge, +4.0, of the ion. Other possible forces have a negligible influence.

(2) Bosvieux and Friedel[48] and Gerl[49] recently theorized that the interstitial atom can not feel the field force. In this case, the transport of carbon in γ iron can only be explained by the existence of a "hole wind" which drives the carbon atoms by momentum transfer towards the cathode. This theory fails to explain why Z^* is exactly +4.0 for carbon in γ iron, and also appears inconsistent with the fact that changing the electron-to-atom ratio (by changing the carbon content of the steel) does not change the magnitude of the force exerted by the electronic carriers. In the present experiments no concentration dependence of Z^* was found by analyzing the results for 0.11 and 0.47% carbon steels.

(3) If, as deduced by Huntington,[50] the charge on the carbon ion is partially screened, then the total force on the carbon atom is the sum of the field force plus momentum transfer from electronic carriers. The same objections apply to this explanation as to (2).

As shown in Table 2.1, the previous investigators of electrotransport of carbon in iron obtained widely scattered values for Z^*. The range was from +1.4 to +13.5 for temperatures from 950° to 1,400°C, carbon contents from 0.4 to 1.1 wt. %, and a current density of about 2,000 A/cm^2. The present result shows no effect of temperature, carbon content, or current density on the Z^* value of +4.0.

CHAPTER VIII

SUGGESTIONS FOR FUTURE WORK

Experimental Apparatus and Techniques

Several suggestions concerning the experimental equipment and procedure will be useful for future work. One of the most serious troubles which we encountered was in the Current Modulation Controller, G. E. TYPE 524-001. Because of its lack of stability, the controller response was sometimes very slow compared to the rate of fluctuation of the line voltage and of the contact resistances, both at the graphite/electrode contact and at the plated-specimen/graphite contact. These troubles caused serious difficulties in completing an experiment, by including actual melting of the specimen. Replacement of the controller by a more desirable type with better stability will be necessary for more effective experiments. As mentioned above, the fluctuation in line voltage was sometimes troublesome, so the installation of a constant voltage transformer may be recommended.

It would be desirable, also, to improve the contact between the specimen and the current-applying devices; i.e., the graphite discs or the electrodes. One way to accomplish this purpose would be to apply a light, constant pressure on the electrode using the presently available counterweight.

Extension of the Interstitial Electrotransport Experiment

The results of the present experiment can be explained best by assuming that the predominant force in the electromigration of carbon in γ iron is the field force. It would be interesting to investigate other interstitial systems, such as Fe-N, Fe-H, Fe-O, Fe-B, etc., to find out if they show the same behavior. Furthermore, a substitutional alloying element such as silicon, manganese, etc., might be added to the iron-carbon alloy to change the number of electrons in the conduction band. If electronic conduction is important in the mechanism of interstitial electrotransport, such alloyed specimens should reveal this fact.

A different area of considerable interest involving interstitial systems is the phase transformation from austenite (γ) to ferrite (α) in Fe-C and Fe-X-C, where X represents an alloying element such as nickel. Two recent papers from this Department have considered the α/γ interface in the course of this phase transformation from the viewpoint of chemical diffusion.[51,52] These papers have contributed to the growing consensus that reactions occurring at the α/γ interface can influence the austenite → ferrite transformation, especially when an alloying element is present. It is proposed that an additional flux, caused by electrotransport, be caused to flow across the interface at which the transformation is occurring. By using a sandwich specimen of the type ferrite/austenite/ferrite (at the temperature of the experiment), the additional flux will aid the transformation at one interface and impede it at the other interface. Preliminary experiments have demonstrated the feasibility of this experimental approach.

APPENDICES

APPENDIX I

Solution of Steady-State Equation

The initial form of the equation (where J = 0) is

$$D \frac{dn}{dx} = nUE \quad . \tag{A1.1}$$

Substituting the electrical mobility, U, into Eq. (A1.1),

$$\frac{eZ^*}{kT} E \, dx = \frac{dn}{n} \tag{A1.2}$$

it follows from Eq. (4.14) that,

$$\frac{S}{\ell} dx = \frac{dn}{n} \quad . \tag{A1.3}$$

The solution of Eq. (A1.3) for the condition that $n = n_{min}$ at $x = 0$ is

$$n = n_{min} \, e^{\frac{S}{\ell} x} \tag{A1.4}$$

where n_{min} is the minimum concentration at one end of the specimen. From conservation of mass,

$$\int_0^{\ell} n dx = n_o \ell \tag{A1.5}$$

where n_o is the uniform, initial concentration. The substitution of Eq. (A1.4) into Eq. (A1.5) gives

$$n = \frac{n_o}{(1/S)(e^S - 1)} \, e^{\frac{S}{\ell} x} \quad . \tag{A1.6}$$

In addition to the above, the following convenient equation is also obtained from Eq. (A1.4) by using the boundary condition, $n = n_{max}$ at $x = \ell$,

$$\frac{n_{max}}{n_{min}} = e^{S} \tag{A1.7}$$

where n_{max} is the maximum concentration at the far end of the specimen.

APPENDIX II

Geometry of Counting the Radioactivity

An end-window-type gas-flow counter (Nuclear Chicago 480) was used for detecting β-rays emitted from the specimen. Micromil (150 $\mu g/cm^2$) was used for the window material.

The counting geometry is given in Fig. A2.1. The specimen, mounted in a synthetic resin, was put under the window with the aid of the specimen holder. The distance between the surface of the specimen and the window is 1mm. After removing successive layers of the specimen, the above distance was kept constant by inserting thin glass plates (150 and 200u plate) under the specimen holder.

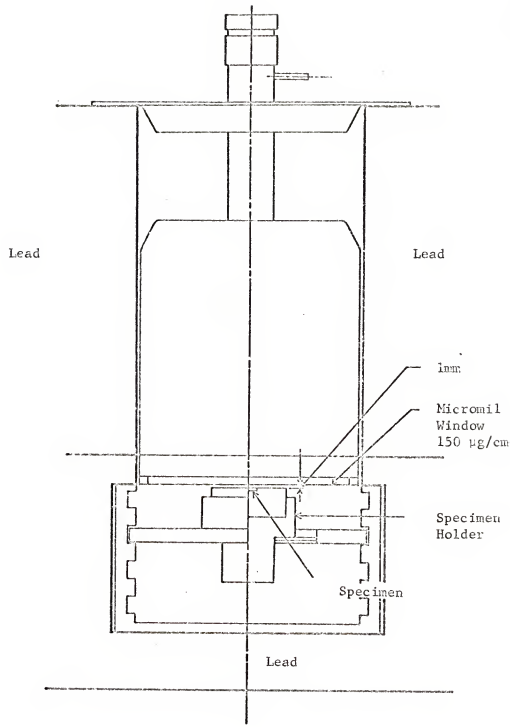

Figure A2.1. Geometry of the measurement of surface activity of the specimen (Nuclear Chicago 480 Gas-Flow Detector).

APPENDIX III

Determination of the Initial Carbon Concentration by a Graphical Method

To convert the carbon-radioactivity vs. distance curve into a carbon composition vs. distance plot after electromigration, it is necessary to evaluate the initial radioactivity. Since it was found that the carbon loss or addition in the specimen during the experiment is negligible, the initial activity was evaluated by the following graphical method. In this determination the surface zone invaded by the coating materials are also considered.

In Fig. A3.1, "a" and "b" represent the diffusion layer and the length of the steel after the experiments, respectively. Therefore, b + 2a represents the initial length of the specimen, which is about 1,000μ. Line (1) is the exponential line obtained from the experimental plots, while line (2) is the straight line drawn so as to obtain the area $A_1 + A_2 = B$, since no carbon loss or addition occurred.

The initial carbon radioactivity, ℓ_I, unknown after the experiment, therefore must be calculated as shown below. The mass-conservation law leads to the following relationship:

$$\ell_I(b+2a) = \ell_1 \times b + \frac{\ell_2 \times b}{2} \qquad \text{(A3.1)}$$

Thus ℓ_I is given by

$$\ell_I = \frac{b}{a + b}\left(\ell_1 + \frac{\ell_2}{2}\right) \qquad \text{(A3.2)}$$

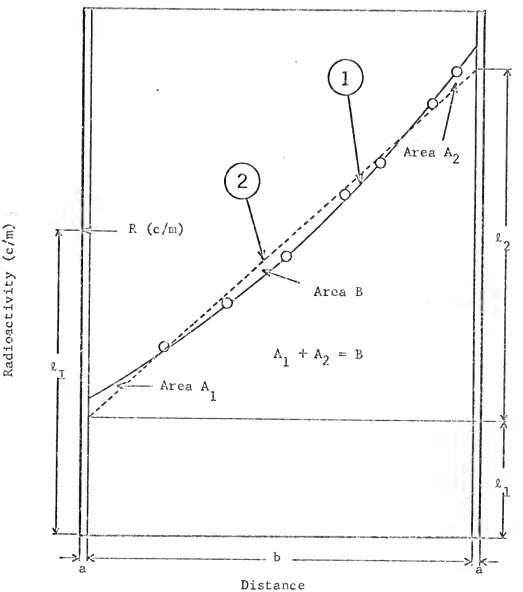

Figure A3.1. Schematic diagram for determining the initial radioactivity by a graphical method.

Since a, b, ℓ_1 and ℓ_2 can be evaluated after the experiment, it is possible to determine the initial radioactivity.

Now, assuming that the labeled carbon atoms, C^{14}, are distributed uniformly among the normal, inactive carbon atoms, the radioactivity vs. distance curve can be converted into a carbon content vs. distance plot using the radioactivity reading, R(c/m), at ℓ_I.

Assuming that the initial carbon content is C (wt. %), the relationship between carbon content and radioactivity is given by

$$y = \frac{C}{R} x \qquad \text{(A3.3)}$$

where y is the carbon content at the position in the specimen where the radioactivity is x(c/m).

LIST OF REFERENCES

1. M. Gerardin, Comp. rend. 53, 727 (1861).

2. V. M. Sidorenko and R. I. Kripyakevich, Fiz. Khim. Mekh. Mater. 4, 335 (1968), 5, 187 (1969), and 5, 191 (1969).

3. Y. Adda and J. Philibert, "La Diffusion dans les Solides," p. 893, Tome II, Presses Universitaires de France, Paris (1966).

4. J. D. Verhoeven, J. Metals 18, 26 (1966).

5. R. A. Oriani and O. D. Gonzalez, Trans. AIME 239, 1041 (1967).

6. W. Seith and O. Kubaschewsky, Z. Electrochem. 41, 551 (1935).

7. J. D. Verhoeven, Met. Reviews 8, 31 (1963).

8. P. Dayal and L. S. Darken, Trans. AIME 188, 1156 (1950).

9. P. Dayal and L. S. Darken, Trans. Indian Inst. Metals 7, 241 (1953).

10. I. N. Frantsevich et al., Soviet Phys. Solid State 1, 58 (1959).

11. I. N. Frantsevich et al., UNESCO/NS/RIC/29, 194 (1957).

12. I. F. Babikova and P. L. Gruzin, Fiz. Met. Metalloved. 5, 255 (1957).

13. D. F. Kalinovich, Soviet Phys. Solid State 3, 812 (1961).

14. I. I. Kovenskii, Soviet Phys. Solid State 5, 1036 (1963).

15. D. F. Kalinovich et al., Fiz. Met. Metalloved. 23, 366 (1967).

16. M. J. Bibby et al., Can. J. Phys. 44, 2375 (1966).

17. Y. Adda and J. Philibert, "La Diffusion dans les Solides," p. 919, Tome II, Presses Universitaires de France, Paris (1966).

18. M. J. Bibby and W. V. Youdelis, Can. J. Phys. 44, 2363 (1966).

19. W. Seith, "Diffusion in Metallen," p. 254, Springer, Berlin (1955).

20. Th. Heumann, "The Physical Chemistry of Metallic Solutions and Intermetallic Compounds," Vol. 1, H. M. Stationery Office, London (1959).

21. Th. Hehenkamp, Acta Met. 14, 887 (1966).

22. O. N. Carlson et al., J. Less-Common Metals 10, 1 (1966).

23. W. Seith and Th. Daur, Z. Electrochem. 44, 256 (1938).

24. O. D. Gonzalez and R. A. Oriani, Trans. AIME 233, 1878 (1965).

25. C. Wagner and G. Heller, Z. Phys. Chem. 46, 242 (1940).

26. J. H. deBoer and J. D. Fast, Rec. Trav. Chim. 59, 161 (1940).

27. F. Claisse and H. P. Konig, Acta Met. 4, 650 (1956).

28. D. T. Peterson et al., Trans. AIME 236, 1311 (1966).

29. J. C. Warner, U. S. Atomic Energy Comm. Rep., IST-133 (1966).

30. D. T. Peterson and F. A. Schmidt, J. Less-Common Metals 18, 11 (1969).

31. D. T. Peterson et al., Ames Laboratory of the U. S. Atomic Energy Commission, Contribution No. 1873.

32. F. A. Schmidt and J. C. Warner, J. Less-Common Metals 13, 493 (1967).

33. F. K. Tkachenko, Liteinoe Proizvodstvo, No. 11, 37 (1963).

34. D. F. Kalinovich et al., Metalloved. i Term Obrabotka Met., No. 12, 46 (1964).

35. S. R. DeGroot, Physica 9, 699 (1942).

36. C. Wells et al., Trans. AIME 188, 553 (1950).

37. C. S. Lees, J. Iron Steel Inst. 205, 329 (1967).

38. ASTM Standard B242-54 or "Metal Finishing Guidebook," Metals and Plastics, New Jersey (1969).

39. J. Fischer and W. Schmidt, Z. Erzbergbau Metallhuttenw. 9, 284 (1956).

40. G. R. Speich et al., Paper in the Symposium Volume, "Electron Probe Microanalysis," John Wiley, New York (1966).

41. D. E. Thomas and C. E. Birchenall, J. Metals 4, 867 (1952).

42. A. Kohn, Met. Reviews 3, 141 (1958).

43. G. Bruggeman and A. Kant, Int. Jour. Applied Radiation and Isotopes 18, 539 (1967).

44. R. L. Loevinger and M. Berman, Nucleonics 9, 26 (1951).

45. G. D. Chase and J. L. Rabinowitz, "Principles of Radioisotope Methodology," Burgers Pub. Co., Minn. (1966).

46. Nuclear Chicago Technical Bulletin, No. 14, Nuclear Chicago Corp., Ill. (1962).

47. Y. Beers, "Introduction of the Theory of Error," Addison-Wesley Pub. Co., Mass. (1962).

48. C. Bosvieux and J. Friedel, J. Phys. Chem. Solids 23, 123 (1962).

49. M. Gerl, J. Phys. Chem. Solids 28, 725 (1967).

50. H. B. Huntington, private communication.

51. H. Oikawa et al., ASM Trans. Quarterly 61, 110 (1968).

52. A. G. Guy and H. Oikawa, Trans. AIME 245, 2293 (1969).

BIOGRAPHICAL SKETCH

Toru Okabe was born in Tokyo, Japan, on March 24, 1934, and is the oldest of the three children of Teiko and Isao Okabe. He lived mostly in Yokohama and Tokyo, Japan. He graduated from Kanto Gakuin High School, Yokohama, Japan, in March, 1952. In March, 1957, he received the degree of Bachelor of Engineering in Metallurgical Engineering from Waseda University, Tokyo, Japan. After receiving this degree he worked in Japan for about ten years for one of the leading non-ferrous smelting and refining companies in Japan, the Nippon Mining Company, Ltd. He had a position of responsibility and wrote numerous reports on technical projects which he directed. In August, 1966, the company sponsored his graduate studies at the University of Florida after learning of his strong desire to study the recent and advanced materials sciences in the United States. From that time to the present, he was employed as a graduate assistant in the Department of Metallurgical and Materials Engineering, where he completed the requirements for the degree of Doctor of Philosophy and performed research in the field of electrotransport of metals under the guidance of Dr. A. G. Guy.

Toru Okabe is married to the former Masako Amatsuji, and is the father of two girls, Atsuko and Junko. He is a member of Alpha Sigma Mu, the American Society for Metals, and the American Institute of Mining, Metallurgical and Petroleum Engineers.

This dissertation was prepared under the direction of the chairman of the candidate's supervisory committee and has been approved by all members of that committee. It was submitted to the Dean of the College of Engineering and to the Graduate Council, and was approved as partial fulfillment of the requirements for the degree of Doctor of Philosophy.

December, 1969

Robert E. Uhrig
Dean, College of Engineering

Dean, Graduate School

Supervisory Committee:

Chairman

R. E. Fennel

R. T. Duffy

John Thomson